A *MIOPETAURISTA* (SCIURIDAE, RODENTIA) CRANIUM FROM THE MIDDLE MIOCENE OF BAVARIA (GERMANY) AND BRAIN EVOLUTION IN FLYING SQUIRRELS

by MONTSERRAT GRAU-CAMATS[1], ORNELLA C. BERTRAND[2]*, JÉRÔME PRIETO[3], SERGI LÓPEZ-TORRES[4,5,6], MARY T. SILCOX[7] *and* ISAAC CASANOVAS-VILAR[1]*

[1] Institut Català de Paleontologia Miquel Crusafont, Universtitat Autònoma de Barcelona, Edifici Z, Carrer de les Columnes, s/n, E-08193 Cerdanyola del Vallès, Barcelona, Spain; e-mails: montse.grau@icp.cat, isaac.casanovas@icp.cat

[2] School of GeoSciences, University of Edinburgh, Grant Institute, King's BuildingsJames Hutton Road, Edinburgh, EH9 3FE, Edinburgh, Scotland, UK; e-mail: ornella.bertrand@ed.ac.uk

[3] Department für Geo- und Umweltwissenschaften, Paläontologie, Ludwig-Maximillians-Universität München, Richard-Wagner-Str. 10, 80333 Munich, Germany; e-mail: j.prieto@lrz.uni-muenchen.de

[4] Institute of Evolutionary Biology, Faculty of Biology, Biological and Chemical Research Centre, University of Warsaw, Żwirki i Wigury 101, 02-089 Warsaw, Poland; e-mail: s.lopez-torres@uw.edu.pl

[5] Division of Paleontology, American Museum of Natural History, 200 Central Park West, 10024 New York, NY, United States of America

[6] New York Consortium in Evolutionary Primatology, The Graduate Center, CUNY, 365 Fifth Avenue, 10016 New York, NY, United States of America

[7] Department of Anthropology, University of Toronto Scarborough, Toronto, ON, M1C 1A4, Canada; e-mail: mary.silcox@utoronto.ca

*Corresponding authors

Abstract: Flying squirrels (Sciurinae, Pteromyini) are the most successful group of gliding mammals. However, their fossil record mostly consists of isolated dental remains which provide very limited insights into their paleobiology and evolution. Only recently, the first skeleton of a fossil flying squirrel, belonging to the species *Miopetaurista neogrivensis*, has been described. It presents all the diagnostic gliding-related postcranial features of its extant relatives and shows that this group has undergone very little morphological change for almost 12 million years. However, the associated cranium is badly crushed, so particular details of the cranial morphology cannot be described. Here we describe a well-preserved cranium of the closely-related *Miopetaurista crusafonti* from 12.5–12.0 Ma from Bavaria (Germany). Its cranial morphology is found to be almost identical to extant large flying squirrels, even in details such as the position of the foramina. The virtual endocast also shows close affinities to living large flying squirrels in morphology and in the relative volume of different brain regions, showing diagnostic features such as the size reduction of petrosal lobules and olfactory bulbs. However, the encephalization quotient (EQ) and neocortical ratio are lower than observed in extant flying squirrels. EQ is known to increase through time in squirrels, but might also be related to locomotion, as arboreal and gliding squirrels display higher EQs than terrestrial ones. Because *Miopetaurista* was certainly a glider, its comparatively lower EQ and neocortical size support the existence of an independent trend of increasing EQ and neocortical complexity in this flying squirrel subclade.

Key words: Rodentia, Sciuridae, Pteromyini, cranial morphology, endocast, encephalization quotient

INTRODUCTION

Gliding has independently evolved multiple times in mammals. There are at least two different groups of Mesozoic gliding mammaliaforms (volaticotheres and haramyidians; see Meng *et al.* 2006; Han *et al.* 2017; Luo *et al.* 2017), several gliding marsupials (acrobatids, pseudocheirids, petaurids), the colugos (dermopterans), and at least four different rodent families (Jackson 2012; Jackson & Thorington 2012). Gliding rodents include the extant flying squirrels (pteromyins); the scaly-tailed flying squirrels (anomalurids); at least one species of the completely extinct eomyid family from the late Oligocene of Germany (Storch *et al.* 1996); and one extinct dormouse (glirid) species from the Late Miocene of France (Mein & Romaggi 1991). However, of all gliding mammals, only flying squirrels have achieved a significant diversity and wide geographical distribution, being present in all northern continents. For a long time considered to belong to a family or subfamily of their own (Simpson 1945; McKenna & Bell 1997) molecular analyses have shown that they are indeed a tribe (Pteromyini) within the Holarctic tree squirrels (Sciurinae) (Mercer & Roth 2003; Herron *et al.* 2004; Steppan *et al.* 2004; Casanovas-Vilar *et al.* 2018; see Fig. 1). Even though transitional forms have yet to be found, flying squirrels certainly evolved from tree squirrels and all share specialized wrist anatomy to support and extend the patagium (Thorington 1984; Thorington & Darrow 2000; Thorington *et al.* 2002).

Until very recently the fossil record of flying squirrels (Sciurinae, Pteromyini) consisted solely of isolated cheek teeth and a few mandibular and maxillary fragments (see discussion in Casanovas-Vilar *et al.* 2018). Their identification was (and for most of them still is) controversial since many of the dental diagnostic characters used to

recognize extinct flying squirrels are also present in non-gliding species (Thorington *et al.* 2005). This has led to major disagreements regarding the time of divergence and diversification of the group. While for most mammal clades molecular-based estimates yield older dates than those based on the fossil record (for example for the origin of placental mammal orders; e.g., Springer *et al.* 2003; Bininda-Emonds *et al.* 2007; O'Leary *et al.* 2013; Murphy *et al.* 2021), for flying squirrels fossil evidence (specifically isolated cheek teeth belonging to the species *Hesperopetes thoringtoni*) unusually suggested a much older divergence time (ca. 36 Ma; Emry and Korth, 2007) than most molecular phylogenies (ca. 23 Ma; Mercer and Roth, 2003; Steppan *et al.* 2004). Contrary to dental material, postcranial bones are unassailably diagnostic for the group since they are shaped by the anatomical adaptations related to gliding (Thorington 1984; Thorington & Darrow 2000; Thorington *et al.* 2002, 2005). The recent description of a partial skeleton of *Miopetaurista neogrivensis* from the Middle/Late Miocene (11.6 Ma) of Catalonia, Spain, showed that this taxon, previously tentatively assigned to flying squirrels based on cheek tooth morphology, displayed the gliding-related postcranial features observed in extant forms (Casanovas-Vilar *et al.* 2018). Its diagnostic wrist anatomy further revealed that *M. neogrivensis* belonged to the subtribe Pteromyina, which today includes large flying squirrels, implying that the two flying squirrel subtribes (Pteromyina and Glaucomyina) had already diverged at that time (Fig. 1). Moreover, it allowed for a recalibration of estimates of flying squirrel divergence time, resulting in an older time frame (late Oligocene, 31–25 Ma instead of 25–20 Ma). This new estimate is further consistent with the age of some of the oldest purported pteromyinan fossils. Perhaps even more importantly, this fossil showed that flying squirrels are a morphologically conservative group. Total evidence phylogenetic analyses recognized *Miopetaurista* as the sister taxon of the extant giant flying squirrel (*Petaurista*; Casanovas-Vilar *et al.* 2018;

see Fig. 1), with the two genera showing numerous similarities in cranial morphology and a virtually identical postcranial anatomy. The only marked differences were found in the cheek tooth morphology, but the striking morphological similarities in the postcranial skeleton show that giant flying squirrels have undergone little evolutionary change for at least 12 million years so they could be well regarded as 'living fossils'. Phylogenetic analyses combining morphological and molecular data showed that flying squirrels radiated during the Miocene (mostly between 18 and 15 Ma; Casanovas-Vilar *et al.* 2018), with several genera reported from Eurasia and North America (Jackson & Thorington 2012; Casanovas-Vilar *et al.* 2018). However, the attribution of all these taxa to the flying squirrel clade (excepting *Miopetaurista*) is questionable until more diagnostic material (i.e., certain postcranial elements, particularly wrist bones related to the extension of the patagium) is found.

The remarkably complete *Miopetaurista* skeleton recently found in Catalonia included an associated skull, and an additional second cranium was also recovered from a nearby site. Both crania are mostly complete, but one is crushed laterally and the second one dorso-ventrally, so the skull of *M. neogrivensis* was virtually reconstructed using elements from both specimens that were scaled and repositioned. Even though those two crania were CT-scanned, the internal morphology proved difficult to reconstruct and was therefore not considered by Casanovas-Vilar et al. (2018). Here we describe a partial cranium from the late Middle Miocene (12.5–12.0 Ma, see below) of Gumpersdorf near Marktl (Bavaria, Germany) attributed to *Miopetaurista crusafonti*, a closely related species. The cranial cavity was infilled with sediment, which created a natural endocast that is partly exposed in the fossil. By means of CT-scanning we were able to reconstruct a virtual endocast of this specimen and observe in detail endocranial morphological features. Even though there are a few studies that comprehensively describe endocranial

morphology of some Oligocene sciurids (Bertrand *et al.* 2017, 2018), this is the first time a fossil flying squirrel endocast is studied. The aims of this work are twofold. On the one hand it provides an accurate description of the external and internal cranial morphology for the genus *Miopetaurista* based on a well-preserved, uncrushed specimen, and thus completing and significantly improving that of Casanovas-Vilar *et al.* (2018). On the other hand, the endocast is accurately described and compared to that of other extant flying squirrels to reveal if diagnostic brain features are also present. Locomotor mode has been previously related to overall relative brain size and the size of the different brain regions in sciurids (Bertrand *et al.* 2017, 2018, 2019*a*, 2021), although this is debated because of the existence of temporal trends in relative brain size in rodents (i.e., encephalization quotient; Bertrand *et al.* 2019*a*). Since *Miopetaurista* was certainly a glider as its extant relatives, we finally discuss whether locomotion or these temporal trends had a greater impact on brain size and in the relative size of the different brain regions.

MATERIAL AND METHODS

Material, provenance and chronology

The described cranium (Figs 2–5, Appendix S1) was found isolated in 1978 in a gravel quarry at the Gumpersdorf site (near Marktl, Bavaria, Germany), located in the North Alpine Foreland Basin (NAFB) or Molasse Basin, situated on the northern side of the Alps. The NAFB is a large foreland basin, 1000 km long by a maximum width of 130 km, that expands from western France to Austria. It formed during the uplift of the Alps and served as a sink for the sediments eroded from that mountain range (Abdul Aziz *et al.* 2010). In the German part of the basin, the sedimentary infill is divided into five main depositional units: the Lower Marine Molasse (early and middle Oligocene); the Lower

Freshwater Molasse (late Oligocene to Early Miocene); the Upper Marine Molasse (Early Miocene); the Upper Brackish-water Molasse (Early Miocene); and the Upper Freshwater Molasse (OSM: Obere Süßwassermolasse; Middle to Late Miocene; Prieto and Rummel, 2016). The Gumpersdorf site is situated in eastern Bavaria, in the OSM unit, although its correlation to the OSM local biozones (Prieto & Rummel 2016) is uncertain. The cranium was found 2–3 meters below a marl layer, within reworked sediments, that has yielded a diverse paleoflora (Gregor 1982).

The age of these deposits is not well constrained because of the lack of biostratigraphically informative fossils. However, Gumpersdorf had been tentatively correlated to Mammal Neogene (MN) zone MN9 (early Vallesian, 11.2–9.9 Ma; MN zone ranges after Hilgen *et al.* 2012) assuming a chronological proximity to Marktl, a richer site located only a few kilometres to the southwest (Mayr, 1979 and references therein). However, recent biostratigraphic studies (Prieto & Rummel 2016) propose a late MN7+8 (late Astaracian, 13.1/12.6–11.2 Ma) age for Marktl. Another key mammal locality of the uppermost OSM is Hammerschmide, which is correlated to the Middle/Late Miocene boundary (11.6 Ma) on the basis of detailed bio- and magnetostratigraphic data (Kirscher *et al.* 2016). Lithostratigraphic data indicate that Gumpersdorf is a little older than both Marktl and Hammerschmiede, so an age of 12.5 to 12.0 Ma seems a realistic approximation. Therefore, the Gumpersdorf specimen is slightly older than the skeleton of *M. neogrivensis* recovered at Abocador de Can Mata site ACM/C5-D1 (Casanovas-Vilar *et al.* 2018).

This specimen was briefly described and figured by Fahlbusch (1979) who tentatively attributed it to *Miopetaurista crusafonti*. It is curated in the SNSB-Bayerische Staatssammlung für Paläontologie und Geologie, (Munich, Germany) with collection number 1978 V 1.

Three-dimensional data acquisition and reconstruction

The specimen was scanned using a Nanotom M (Phoenix X-ray) micro-CT scanner at the Staatliche Naturwissenschaftliche Sammlungen Bayerns – Zoologishe Staatssammlung Museum (Munich, Germany). Scanning parameters used were 130 kV and 120 mA, including 1505 slices with a voxel size of 32 μm. Raw data were imported to Avizo 8.0.1 software for segmentation and visualization. Cranial bones and endocast were segmented separately using semiautomatic thresholding tools to remove sediment and bone, respectively (Figs 4–5).

Comparative sample

Cheek teeth measurements of the studied specimen were compared to those of other *Miopetaurista* species taken from the literature (Table 1; Grau-Camats *et al.* 2021, table S1). Cranial anatomy and measurements were compared to original specimens (IPS56468h, IPS88677) and to the virtual reconstruction of *M. neogrivensis* (Casanovas-Vilar *et al.* 2018: Fig. 4B) as well as to a representative sample of extant flying squirrels (Fig. 6, Table 2). These comprise the extant Pteromyina *Petaurista petaurista* (ZMA 131418), *Eupetaurus cinereus* (RMNH 19524), *Aeromys tephromelas* (24670), *Belomys pearsonii* (RMNH 56.046) and *Pteromys volans* (RMNH 40035), and the extant Glaucomyina represented by *Hylopetes sagitta* (RMNH 15512), *Glaucomys volans* (RMNH 19786), *Glaucomys sabrinus* (IPS60584) and *Iomys horsfieldii* (RMNH 15937). All specimens of the extant species are housed in the Naturalis Biodiversity Center (Leiden, the Netherlands), except for *G. sabrinus* which comes from the collections of the Institut Català de Paleontologia Miquel Crusafont (ICP). The *M. neogrivensis* original specimens are also curated at the ICP.

193 The virtual endocast of *M. crusafonti* was compared to already published rodent
194 endocasts (Bertrand *et al.* 2016*a*, 2017, 2018, 2019*b*; Bertrand & Silcox 2016; Grau-
195 Camats *et al.* 2021, tables S2–S4; Fig. 8). These include two extant flying squirrels
196 belonging to different subtribes: *Pe. petaurista* (USNM 589079; Fig. 8A) and *G. volans*
197 (AMNH 240290; Fig. 8B). Extinct squirrels are represented by *Cedromus wilsoni*
198 (Cedromurinae; USNM 256584; Fig. 8C) from the Orellan (late Oligocene) of the White
199 River Formation (Wyoming, USA); and the early tree squirrel *Protosciurus* cf. *rachelae*
200 (Sciurini, Sciurinae; YPM 14737; Fig. 8D) from late early Arikareean (late Oligocene–
201 early Miocene) of the John Day Formation (Oregon, USA). The ischyromyid *Paramys*
202 *delicatus* (Paramyinae; AMNH 12506; Fig. 8E) from the Bridgerian (middle Eocene) of
203 the Wind River Formation (Wyoming, USA) as well as other previous published virtual
204 endocasts of Ischyromyidae are also included (Bertrand *et al.* 2019*b*). The inclusion of
205 ischyromyids in our study is crucial. Phylogenetic relationships among the Ischyromyidae
206 and with other rodent groups are still debated, but *Paramys* is generally regarded as one
207 of the most basal rodents (e.g., Korth 1994; Meng *et al.* 2003; Asher *et al.* 2019) . Indeed,
208 this group of rodents has a conservative endocranial morphology (Bertrand *et al.* 2019*a*)
209 and is therefore a good representation of the plesiomorphic state for rodents and in this
210 case for squirrels. Aplodontiidae, is the sister group to Sciuridae (e.g., see Fabre *et al.*
211 2012), for which fossil endocasts are known. However, these belong to *Prosciurus*
212 (Bertrand *et al.* 2018) and *Mesogaulus* (Bertrand *et al.* 2021), dating back to the
213 Oligocene and Early Miocene, respectively, and are already too derived to provide
214 information on the ancestral condition from which sciurids evolved, so they are not
215 considered here. Phylogenetic relationships among the considered taxa, as well as their
216 age is illustrated in Fig. 1.

217 *Anatomical terminology and measurement methods*

Dental terminology and measurement methods for squirrel cheek teeth follow Casanovas-Vilar *et al.* (2015) and references therein. For cranial anatomy, especially cranial foramina, Wahlert (1985, 2000), Wible (2008), Sinitsa *et al.* (2019) and Wible and Shelley (2020) were used as primary references. The description of muscular insertion areas follows Ball and Roth (1995). Linear cranial measurements are after Nicolas *et al.* (2008) and Bertrand *et al.* (2016b) and were taken on physical specimens. Endocast morphology as well as linear and surface measurements follow Bertrand *et al.* (2016*a*, 2017, 2018, 2019*b*) and Bertrand and Silcox (2016). Endocranial volumes and surface areas for extant and fossil squirrels and other rodents are taken from Bertrand *et al.* (2016*a*, 2017, 2018, 2019*b*, 2021). Endocast and brain region volumes were calculated using Avizo, 8.0.1. Because the right side of the endocast is missing a significant portion, the total endocast volume was calculated by doubling the volume of the left half of the endocast. The endocast exhibits some deformation, so it was divided by digitally cutting it between the olfactory bulbs, along the superior sagittal sinus, and the midline of the vermis in dorsal view using the 'volume edit' module. The neocortical surface area was estimated by selecting the area above the orbitotemporal canal on the left side of the endocast only, and excluding the circular fissure and the confluence of sinuses (=NS1; following Jerison 2012; Long *et al.* 2015). The rhinal fissure represents the separation existing between the paleo- and the neocortex (Martin 1990). The relationship between the rhinal fissure and the orbitotemporal canal in rodents exists as in many other mammalian orders (e.g., lemurs; Martin 1990). In the illustration of the brain of *Sciurus vulgaris* (Brauer & Schober 1970), the rhinal fissure is in the same location as the orbitotemporal canal in the virtual endocast of *Sciurus carolinensis* (Bertrand & Silcox 2016: Fig 7c). The selected area in this hemisphere was then doubled. Because the right side is damaged, the total endocranial surface (TS), which includes the olfactory bulb

length (see Bertrand & Silcox 2016) was estimated by using the left side only as well and doubling it. Volume and surface area ratios are expressed as percentages.

Body mass and encephalization quotient estimations

Body mass (BM) was estimated using a linear regression of body mass vs. cranial length computed with the software R version 4.0.2 (R Core Team 2020) following the methods of Bertrand *et al.* (2016a). The encephalization quotient (EQ) was used to compare endocranial volume among species with different body masses. The EQ equation used [$EQ = 0.0097\ (BM)^{0.06419}$] was the one proposed by Pilleri *et al.* (1984), which is specifically adapted to rodents. Statistical tests and plots were made using R version 4.0.2 (R Core Team 2020). For comparison purposes, we included the EQ produced by Eisenberg and Wilson (1978).

Phylogenetic signal analysis

We performed regressions on the endocranial data using Phylogenetic Generalized Least Squares (PGLS) regressions (Grafen & Hamilton 1989). The regressions were calculated and plotted using R version 4.0.2 (R Core Team 2020). To perform the PGLS analyses, we used the tree topology proposed by Bertrand *et al.* (2021), based on Korth and Emry (1991) and Mercer andRoth (2003), with the addition of *M. crusafonti* as sister taxon of *Petaurista* following Casanovas-Vilar *et al.* (2018). The phylogenetic tree used is given in Fig. 1. We used Bayesian method to time calibrate our tree with the function "createMrBayesTipDatingNexus" in the paleotree package v3.3.25 (Bapst 2012) and followed the protocol of Bapst (2013, 2014) to create a script that was subsequently ran in the software MrBayes (v3.2.7; Huelsenbeck & Ronquist 2001; Ronquist & Huelsenbeck 2003). We employed the "gls" function of the nlme package (version 3.1-142) to run the PGLS analysis (Pinheiro *et al.* 2020) and used the Lambda model

(Brownian motion with internal branches multiplied by Pagel's λ [lambda]; Pagel 1999). We obtained a total of six final PGLS regressions: (1) endocranial volume in relation to body mass, (2) petrosal lobule volume in relation to body mass, (3) olfactory bulb volume in relation to body mass, (4) neocortex surface area in relation to endocranial surface area, (5) petrosal lobule volume in relation to endocranial volume, (6) olfactory bulb volume in relation to endocranial volume. We computed Pagel's λ (Pagel 1999) for each PGLS regression, a scaling coefficient that detects whether the shared evolutionary histories as specified by the phylogeny are responsible for the patterns of similarity observed in the data. Values below 1 correspond to traits being less similar amongst species than expected from their phylogenetic relationships, while values above 1 suggest the reverse. We also provide the 95 % confidence intervals for each PGLS regression following the recommendations from Symonds & Blomberg (2014).

We generated the predicted and residual values for each PGLS regression using the function "predict" and "residuals" from the stats package (version 3.6-2). The functions "R2.pred" and "R2.lik" from the rr2 package (version 1.0-2) were used to generate the coefficient of correlation for each regression. We decided to report two different estimates of the coefficient of correlation using the R^2 obtained from the predicted and from the residual values. The first one is better than other R^2 estimators in determining how much variation is explained by the model, while the second one is more useful when assessing the significance of each variable used in the model (Ives 2019).

Institutional abbreviations. AMNH, American Museum of Natural History, New York, USA; IPS, Institut Català de Paleontologia Miquel Crusafont, Sabadell, Spain; RMNH, Naturalis Biodiversity Center, Leiden, the Netherlands; SNSB, Bayerische Staatssammlung für Paläontologie und Geologie, Munich, Germany; USNM, National Museum of Natural History, Smithsonian Institution, Washington, D.C., USA; YPM,

Peabody Museum of Natural History, Yale University, New Haven, USA; ZMA, Zoological Museum of Amsterdam collection, Naturalis Biodiversity Center, Leiden, the Netherlands.

DESCRIPTIONS AND COMPARISONS

Cheek tooth morphology

The upper cheek teeth show smooth enamel without lophules; the ridges are relatively simple and thick (Fig. 3E). The metaloph and the protoloph are parallel and do not converge towards the protocone. The posteroloph and anteroloph are lower than the protoloph and metaloph. The protocone is longitudinally elongated. The P4–M3 have a large, antero-posteriorly elongated root under the protocone and two smaller cylindrical roots below the metacone and paracone.

P3. It is small and conical, with a single cylindrical root. It has a prominent anterior cusp and a posterior ridge which encloses a small basin. A small posterior cusp is present on the posterior ridge.

P4. The right P4 is missing. The left one is subtriangular, longer than wide, and with a well-developed anterior region. There are three main cusps: metacone, paracone and protocone. The hypocone is reduced and integrated into the endoloph, although this cusp is more marked than on the molars. The mesostyle is evident and closes the central valley. The parastyle is labio-lingually elongated and is as large as the main cusps and only slightly less prominent. There are two longitudinal spurs that weakly connect the metaloph with the posteroloph. The anterior valley is relatively wide and labially open, while the posterior one is very narrow.

315 *M1/M2*. Both molars are subrectangular, their width is notably greater than their length.
316 The M2 is relatively longer and squarer than the M1. Each of these molars possesses three
317 main cusps: metacone, paracone and protocone. The M1 has a diminutive mesostyle,
318 whereas it is missing in the M2. The protoloph is constricted near the point where it
319 merges with the protocone. The central valley is wide and labially open. In both molars
320 the metaloph shows a tiny posterior spur that just reaches the posteroloph but does not
321 merge with it. The anterior and posterior valleys are open, the latter being much narrower.
322 *M3*. It is subtriangular, with a conspicuously narrower posterior half. This tooth has two
323 main cusps: paracone and protocone. The metacone is reduced to a small cusp integrated
324 into a ridge that defines the posterolabial border of the molar. There is a highly reduced
325 postero-lingual valley defined by a thin and arched ridge, presumably corresponding to
326 the metaloph. This minute valley is partially closed by a small cingulum descending from
327 the labial side. As described for the other molars, the protoloph is constricted near the
328 point where it merges with the protocone. The anterior valley is very narrow and shallow
329 while the central valley is wider and deeper. Both valleys are labially open. Cheek teeth
330 measurements are given in Table 1 and comparisons are given in Grau-Camats *et al.*
331 (2021, table S1).
332 *Comparisons and species attribution.* The Gumpersdorf specimen is assigned to the genus
333 *Miopetaurista* because of its large size; the absence of enamel crenulations on the upper
334 cheek teeth; and the protoloph and metaloph of P4–M2 lacking conules and being parallel
335 to one another rather than lingually convergent (Mein 1970; Daxner-Höck & Mein 1975;
336 de Bruijn 1999). The specimen belongs to a medium-sized *Miopetaurista* species, clearly
337 larger than the Early Miocene species (early to middle Orleanian, MN3–MN4)
338 *Miopetaurista diescalidus*, *Miopetaurista dehmi* and *Miopetaurista lappi*. It further
339 differs from these species by the absence of a mesoloph, and from *M. diescalidus* in

particular by the different shape of the P4, which presents a characteristically reduced and more rounded P4 (Daams 1977). In the case of *Miopetaurista gibberosa* from the Middle Miocene (late Orleanian, MN5) of Göriach (Austria), only lower cheek teeth are known (Daxner-Höck & Höck 2015), but these clearly belong to a smaller species. Younger species include *Miopetaurista neogrivensis* (late Astaracian to early Vallesian, MN7+8–MN9) and *Miopetaurista thaleri* (late Turolian to Villanyan, MN13–MN16), which are the largest species of the genus, rivalling in size the extant giant flying squirrels of the genus *Petaurista* (see Casanovas-Vilar *et al.* 2018). The material from Gumpersdorf is slightly smaller than that ascribed to these two species and the shape of the P4 is more triangular, being markedly narrower in its lingual part. In addition, the morphology of the upper cheek teeth is more complex in *M. thaleri*, the M1/M2 always having a short anterior spur in the protoloph (Mein 1970).

The Gumpersdorf material closely matches the size of the species *Miopetaurista gaillardi* (Astaracian, MN6–MN7+8) and *Miopetaurista crusafonti* (Vallesian to early Turolian, MN9–MN11), although it is closer to the latter. The former is known from several sites ranging from Portugal to Turkey while the latter has previously only been reported from Catalonia and southern France (Casanovas-Vilar *et al.* 2015). The described material is slightly larger than *M. gaillardi*, further differing in the shape of the P4, which is more triangular and presents a well-developed parastyle as in *M. crusafonti*. Other aspects of the P4 morphology resemble these two species, such as the presence of a pronounced mesostyle and two short posterior spurs in the metaloph directed towards the posteroloph (see Mein 1970; Casanovas-Vilar *et al.* 2015). In *M. gaillardi* the P4 possesses an additional small cusp between the paracone and the parastyle, which is absent in the Gumpersdorf material and in *M. crusafonti* (Casanovas-Vilar *et al.* 2015). The size and morphology of the described material supports its ascription to *M. crusafonti*

as already suggested by Fahlbusch (1979), even though the M1/M2 may show a more complex morphology in this species, with additional short spurs (Casanovas-Vilar *et al.* 2015). The P3 morphology of *M. crusafonti* is here described for the first time. As compared to *M. neogrivensis* the P3 is more rounded and presents two well-defined cusps. The material of Gumpersdorf confirms the occurrence of *M. crusafonti* in Germany during the latest Middle Miocene (late Astaracian, MN7+8), being the only record of this species in Central Europe. Younger occurrences of the genus *Miopetaurista* in Germany, such as that from Dorn-Dürkheim 1 (early Turolian, MN11), have not been identified to the species level but apparently correspond to a larger-sized species (Franzen & Storch 1975; Franzen *et al.* 2013).

Cranial anatomy and comparisons

Description. The cranium is short and wide (Figs 2–5 and Appendix S1). The total estimated length of the cranium is 67.7 mm from the tip of the snout to the posterior part of the braincase (for cranial measurements and comparisons see Table 2). The rostrum is laterally crushed and deviated towards the right side. It is short and appears to have also been wide, although extensive damage to this region obscures its morphology. The nasals and premaxillary bones are crushed, and the different fragments displaced. The left incisor is missing, but the right one is complete, with only minor damage on its tip. The incisor is clearly orthodont and relatively slender. Only the anteriormost border of the right incisive foramen is preserved, so it is impossible to evaluate its shape and size. The infraorbital foramen is small and rounded. The infraorbital canal is long and opens lateral to the rostrum. The orbital region, particularly the left side, is well preserved. The braincase is not notably deformed or crushed but important parts are missing, particularly in the dorsal part of the cranium (i.e., most part of the frontal and the right parietal; Figs 3–4, Appendix S1). The zygomatic arches are broken, and only the zygomatic process of

390 the squamosal and the ventral half of the zygomatic plate are preserved. Most of the
391 occipital region is crushed, and the right half of the occipital bone is entirely absent. The
392 auditory bullae are missing. The brain cavity is infilled with terrigenous sediment, thus
393 producing an almost complete natural endocast (Fig. 3, Appendix S1).

394 In ventral view, the masseteric tubercles are bulbous and prominent (Fig. 4A). The
395 zygomatic plate is relatively vertical and wide as in other sciurids. A semicircular ridge
396 in front of the cheek teeth marks the insertion area for the anterior portion of the
397 buccinator muscle. The palate is not particularly wide and is pierced by an anterior pair
398 of posterior palatine foramina at the level of the M2. The posterior pair of posterior
399 palatine foramina are just tiny punctures in the maxillary bone close to the suture with the
400 palatine bones. The palatines are pierced by a well-developed, rounded and closed
401 posterior maxillary foramen just posterior to the M3. The posterior margin of the palatines
402 is straight but there is a short and rounded posterior nasal spine. Only the anterior part of
403 the pterygoid ridges is preserved but these appear to have been slightly divergent
404 posteriorly. The left foramen ovale is preserved. It is large, rounded and located
405 anteromedially to the inferred position of the auditory bulla. The lateral flange of the
406 pterygoid encloses the alisphenoid canal, which has moved from its original position. The
407 transverse canal is smaller and medial to the foramen ovale. A fragment of the
408 basisphenoid, a rectangular flat plate, is preserved on the left side.

409 In the orbital region, a rounded and relatively large sphenopalatine foramen is
410 clearly visible in the left side, whereas only its anterior border is preserved in the right
411 side (Fig. 5A). This foramen is located at the level of the anterior edge of the third molar
412 and is mostly included within the maxillary bone. An oval upper ethmoid foramen is well
413 preserved in the left frontal. The lower ethmoid foramen can only be observed in the left
414 frontal and it is somewhat damaged. It is much smaller than the upper foramen and it is

415 located more posteriorly, close to the suture with the squamosal. The posterior part of the
416 orbital region comprising the orbitosphenoid, as well as part of the palatine and frontal
417 bones is damaged, so that the optic and dorsal palatine foramina are not preserved. A
418 large and elliptical masticatory foramen (including the buccinator foramen) is visible on
419 both sides, although it is better preserved on the right side. Medial to the masticatory
420 foramen, the edge of a large sphenorbital fissure can also be recognized on the right
421 alisphenoid. Finally, a small and elliptical postglenoid foramen is visible just below the
422 posterior edge of the posterior zygomatic root. This foramen is only preserved on the left
423 side of the cranium.

424 The postorbital processes are not preserved (Fig. 4B). The interorbital distance is
425 relatively narrow compared to other squirrels (Table 2; see also Fig. 6). Even though the
426 zygomatic arch is broken, its posterior root is preserved on both sides of the cranium. It
427 is robust and almost horizontal (Fig. 4B). The cranial vault looks relatively convex
428 because most of the region of the cranium anterior to it is crushed and poorly preserved
429 (Fig. 5A). When considered in isolation, it appears to have been quite flat, thus resembling
430 *M. neogrivensis*. Only the left half of the parietal is preserved, but it shows a marked
431 temporal ridge for the insertion of the temporalis muscle (Fig. 4B). The posterior half of
432 the ridge curves medially before merging with a marked nuchal crest.

433 As already stated, the auditory bullae are not preserved. Furthermore, the right
434 half of the cranial vault is entirely missing. However, this makes it possible to observe
435 the petrosal, which is well preserved on the left side of the cranium (Fig. 5B, Appendix
436 S1). In medial view, the petrosal crest defines the posterior margin of a large middle
437 cranial fossa that houses the posterior part of the cerebrum (Fig. 2, Appendix S1). A short
438 sulcus on the inner surface of the anterior lamina of the petrosal likely only carried the
439 internal carotid nerve, as the proximal stapedial artery (=transpromontorial portion of the

artery in Wible, 1984) is absent in modern Sciuroidea. Within the alisphenoid bone, the large internal opening of the foramen ovale can also be observed on the anteroventral side of this middle cranial fossa. A smaller posterior depression, the subarcuate fossa, occupies the posterointernal side of the petrosal and would have housed the petrosal lobule (=paraflocculus), part of the cerebellum (Fig. 2, Appendix S1). Ventral and anteromedial to the subarcuate fossa there is a large internal auditory meatus, subdivided by a tiny transverse crest, slightly more recessed than the meatus. The upper fossa of the internal acoustic meatus, namely the superior acoustic foramen, is subdivided by an even weaker crest perpendicular to the transverse crest. This perpendicular crest delimits an anterior round opening into the facial canal and posteriorly a smaller superior vestibular area, as well as a lower opening for the inferior vestibular area. The lower fossa of the internal acoustic meatus, termed the inferior acoustic foramen, is also subdivided by a tiny ridge. Its anterior half has a large and elliptical opening, the spiral cribiform tract. Posterolateral to this foramen, is the much smaller foramen singulare for the posterior ampullary nerve (branch of the vestibulocochlear nerve VIII) to the ampulla of the posterior semicircular canal. The ridge separating the internal acoustic meatus from the subarquate fossa presents a tiny circular foramen, likely the vestibular aqueduct. A small foramen, presumably corresponding to the mastoid foramen (see Wible & Shelley 2020: 6, 29), is located posterodorsally to the subarcuate fossa. Another small foramen pointing towards the back of the cranium is located posteroventrally to the internal auditory meatus. This foramen likely corresponds to the hypoglossal foramen for nerve XII. Finally, two small foramina can be observed at the back of the skull, close together and near the occipital margin. These foramina likely correspond to two condyloid canals.

Comparisons. The cranium is short and wide, resembling that of the large flying squirrels *Aeromys* and *Petaurista* (Fig. 6), further being comparable in size to *M. neogriviensis* and

Pe. petaurista (Table 2). The rostrum is short and was probably broad, as in *Miopetaurista*, *Petaurista* and *Aeromys.* It exhibits orthodont upper incisors as seen in our sample of extant flying squirrels. In palatal view, the masseteric tubercles are bulbous and prominent, being similar to those of *Petaurista*. The zygomatic plate is similar in morphology and size to that of other studied flying squirrels. The infraorbital foramen is small and rounded as in *Petaurista.* The ridge for the insertion of the anterior portion of the buccinator muscle is clearly marked as a semicircular scar similar in shape to that of *Aeromys*. The palate is not particularly wide, being narrower than in Glaucomyina, such as *Glaucomys*, *Hylopetes* and *Iomys*. The shape and width of the palate is again close to *Petaurista*. The posterior palatine foramina are located at the M2 level, in the maxillary bone. This resembles the condition seen in *Aeromys* whereas in other compared extant flying squirrels the palatine foramina are located in the palatine, just in the suture with the maxillary or immediately behind it. The palatines enclose two posterior maxillary foramina, which differ from those of other Pteromyina. These foramina are not completely closed in the studied *Pe. petaurista*, *Eupetaurus cinereus* and *Pteromys volans* as well as in Glaucomyina species. *Aeromys tephromelas* and *Biwamoyopterus laoensis* (see Li *et al.* 2019) are the only studied Pteromyina that show closed posterior maxillary foramina, although they are more elongated in *A. tephromelas* than in *M. crusafonti*. However, the intrageneric and intraspecific variability of this character has not been evaluated, and the foramen is known to be closed in one species of the genus *Biswamoyopterus* (*B. laoensis*) but not in the other two (*B. biswasi*, *B. gaoligongensis*; see Li *et al.* 2019). *Miopetaurista crusafonti* presents a short and rounded posterior nasal spine, similar in shape to that of *Pe. petaurista* and *E. cinereus.* The pterygoid ridges are parallel in our sample of flying squirrels, but in *M. neogrivensis* and apparently in *M. crusafonti* as well they diverge slightly posteriorly. The foramen ovale is large and

relatively close to the anterior margin of the auditory bulla, similar in size and shape to that of large-sized flying squirrels.

The interorbital distance is relatively narrow as compared to our sample of extant Pteromyina (Table 2; Fig. 6). Only *Belomys* and *Pteromys* show a similar interorbital constriction, and the interorbital distance is wider in other Pteromyina including *M. neogrivensis*. In the orbital region the frontal bone is pierced by an oval upper ethmoid foramen at the level of the M3 whereas in other Pteromyina such as *Pe. petaurista* and *A. tephromelas* it is more anteriorly placed, at the level of M2. Glaucomyina also have a more anterior upper ethmoid foramen compared to *M. crusafonti*, at the M2 level. The sphenopalatine foramen is almost entirely included within the maxillary bone, as observed in *A. tephromelas*. However, in extant large flying squirrels, as well as in some small taxa such as *Hylopetes sagitta*, the position of this foramen is more anterior (at the contact between M1 and M2) than in *M. crusafonti* (at the contact between M2 and M3). The squamosal is relatively low and presents a small postglenoid foramen, which within the compared specimens only occur in *Petaurista* and *Eupetaurus*.

The root of the jugal is deep and robust approaching the morphology of *Petaurista*. On initial overview, the cranial vault of *M. crusafonti* seems relatively convex, more closely resembling smaller-sized flying squirrels. However, the dorsal part of the cranium, particularly the frontal, is poorly preserved thus giving this false impression of convexity. Therefore, the morphology of the cranial vault was certainly somewhat originally flatter, although probably not as much as in *Petaurista* or *Aeromys* species. The preserved part of the parietal bone shows a prominent temporal ridge that curves medially towards the nuchal crest similarly to *M. neogrivensis* and *E. cinereus*. These ridges do not come as close towards the posterior side of the cranium in other flying squirrels, such as in *Petaurista*, *Aeromys* or *Pteromys*.

Except for its greater interorbital constriction, the cranium of *M. crusafonti* does not differ significantly from that of *M. neogrivensis* (Fig. 6B), hence being remarkably similar to the large flying squirrels *Petaurista* and *Aeromys*. Yet, as remarked by Casanovas-Vilar *et al.* (2018), the cheek tooth morphology is clearly different and there are subtle cranial differences. *Miopetaurista* has the temporal ridges that converge towards the posterior edge of the cranium, resembling the condition seen in *Eupetaurus*. On the other hand, the morphology of the posterior maxillary foramina is different from that of *Petaurista* and *Aeromys*, but the intrageneric and intraspecific variability of this character has not been assessed, so it may not be diagnostic.

Endocranial anatomy and comparisons

Olfactory bulbs. The olfactory bulbs of *M. crusafonti* are located above the M1 (Fig. 2, Appendix S1), which is different to the position observed in all fossil and extant squirrels but similar to some ischyromyids (see Bertrand *et al.* 2018). It is possible that the position of the olfactory bulbs could have resulted from deformation of the rostral region being telescoped anteriorly compared to the braincase; however better-preserved specimens will be necessary test this hypothesis. In ischyromyid rodents past studies have found that the olfactory bulbs are positioned more posteriorly relative to the toothrow, above the M1–M2 (Bertrand *et al.* 2016*b*, 2019*b*). This might be related to the fact the rostrum appears to have shortened and the braincase expanded due to brain size increase in Sciuridae compared to Ischyromyidae (Bertrand *et al.* 2019*a*). The olfactory bulbs represent 1.2 % of the total endocranial volume in *M. crusafonti* (Grau-Camats *et al.* 2021, table S4). *Miopetaurista crusafonti* has a smaller olfactory bulb volume ratio compared to Eocene and Oligocene Ischyromyidae (3.2 % to 6.1 %), the Oligocene squirrel *Cedromus wilsoni* (3.0 %), the late Oligocene Sciurini *Protosciurus* cf. *rachelae* (3.7 % and 4.9 %), and extant squirrels, which range from 1.6% to 4.7 %. *Miopetaurista*

crusafonti also has a lower ratio compared to extant flying squirrels, which range from 1.6 % to 3.5 % in olfactory bulb ratio (Table 3; Grau-Camats *et al.* 2021, table S4). Among the considered extant squirrel sample, *Ratufa affinis* and *Pe. petaurista*, the closest living relative of *M. crusafonti*, show the lowest olfactory bulb volume ratios (1.6 %). Log-transformed olfactory bulb volume shows a positive and highly significant correlation with both log-transformed endocranial volume and body size (Fig. 9A, B; Table 4). Both endocranial volume and body mass explain a high portion of the variance according to PGLS regression (Table 4; r^2=0.86 against body mass and r^2=0.91 against endocranial volume). The phylogenetic signal is moderate when assessed against body mass (λ~0.6) and high (λ~0.9) if endocranial volume is considered (Table 4). *Miopetaurista crusafonti* has smaller olfactory bulbs than would be expected for its endocranial volume compared to ischyromyids, other fossil sciurids and the majority of extant squirrels (Fig. 9A). It also has smaller olfactory bulbs than would be expected when assessed against body mass compared to extant sciurids (Fig. 9B). The flying squirrels *Pe. petaurista* and *Pteromys buechneri* have high negative residuals and occupy a similar position relative to the regression line for squirrels to *M. crusafonti* (Grau-Camats *et al.* 2021, tables S6–S7) although they fall within the cluster of Ischyromyidae when the comparison is made with respect to body mass (Fig. 9B).

Cerebrum and midbrain. The circular fissure (Fig. 7A, Appendix S1) of *M. crusafonti* is shorter antero-posteriorly than in ischyromyid rodents but similar in length compared to that of sciurids, including the extinct *C. wilsoni* and *Pr.* cf. *rachelae* (Fig. 8; Bertrand *et al.* 2017, 2018, 2019*b*). The ratio of cerebellum maximum width to cerebrum maximum width (CLW/CRMW) is variable in the studied taxa (Grau-Camats *et al.* 2021, table S3). *Miopetaurista crusafonti* has a ratio of 65.8 %, which is very close to the value for the early squirrel *C. wilsoni* (66.2 %) and lower than the values for the two specimens of *Pr.*

565 cf. *rachelae* (69.4 % and 79.27 %). The ratio of *M. crusafonti* is lower than the range
566 observed for extant squirrels (68.8 % to 82.4 %). This result contrasts with the condition
567 in ischyromyids, for which the ratio is higher, between 82.5 % and 103.6 %, suggesting
568 that the cerebellum and cerebrum have more similar widths in this family of early rodents
569 (Bertrand *et al.* 2019*b*). Previous research concluded that the lower ratio exhibited by
570 squirrels is explained by the lateral expansion of the cerebrum relative to the cerebellum
571 compared to the configuration in ischyromyid rodents (Bertrand *et al.* 2018, 2019*b*). The
572 lowest ratios in the extant dataset occur in flying squirrels, with two species displaying
573 the lowest values for extant taxa: *Hylopetes spadiceus* (68.8 %) and *Pt. buechneri*
574 (69.3%). The midbrain is not visible on the endocranial surface of *M. crusafonti*, which
575 implies complete coverage of this area by the cerebrum (Figs 7A, C). The observed
576 condition resembles all extant squirrels (e.g., Fig. 8A–B) but contrasts with the situation
577 in other extinct squirrels which exhibit only a partially covered midbrain (Fig. 8C–D;
578 Bertrand *et al.* 2017, 2019*b*).

579 A temporal fossa is visible in the fossil taxa *C. wilsoni* (Fig. 8C), *Pr.* cf. *rachelae*
580 (Fig. 8D), *M. crusafonti* (Fig. 7C) as well as in all studied extant squirrels. In contrast, the
581 fossa is absent in most ischyromyid rodents (e.g, Fig. 8E) with the exception of
582 *Pseudotomus horribilis*, *Pseudotomus hians*, one specimen of *Ischyromys typus* and in
583 *Reithroparamys sciuroides* (Bertrand *et al.* 2019*b*). The Sylvian fossa is absent in the
584 fossil taxa *M. crusafonti*, *Pr.* cf. *rachelae,* and also in the ischyromyids (Bertrand *et al.*
585 2018, 2019*b*). The presence of this structure is variable among other extant and extinct
586 squirrels. For instance, a Sylvian fossa is visible in *C. wilsoni* (Fig. 8C), but is absent in
587 our sample of pteromyins except for *A. tephromelas*, *Petinomys setosus* and *Pt.*
588 *buechneri*, while an actual Sylvian sulcus can be observed in the invertivorous
589 callosciurine *Rhinosciurus laticaudatus* (Bertrand *et al.* 2017). Lateral sulci are absent in

590 *M. crusafonti*, *C. wilsoni*, *Pr.* cf. *rachelae* and in the majority of our extant squirrel
591 sample, while the presence of lateral sulci is variable in the ischyromyids (see Bertrand
592 *et al.* 2019*a*). However, they are visible in large flying squirrels, such as the pteromyins
593 *A. tephromelas* and *Pe. petaurista* (Fig. 8A; Bertrand *et al.* 2017), which also have the
594 highest endocranial volumes within the Sciuridae (11.5 cm^3 in *A. tephromelas* and 12.3
595 cm^3 in *Pe. Petaurista*; Table 3; Grau-Camats *et al.* 2021, table S4). Calculated endocranial
596 volume for *M. crusafonti* is 10.82 cm^3, thus being lower than both extant taxa. In general,
597 presence or absence of neocortical sulci is related to the endocranial volume, with brains
598 of less than 5 cm^3 generally being lissencephalic (Macrini *et al.* 2007). For rodents, both
599 gyrencephalic and lissencephalic brains can be found in an interval of brain masses
600 between 3 and 30 cm^3 (Pilleri *et al.* 1984). The absence of sulci in all but the largest
601 squirrels suggests that the value below which gyrification occurs may be higher than in
602 some other mammalian groups. As such, *M. crusafonti* may differ from the large extant
603 flying squirrels in lacking the lateral sulcus because of its somewhat smaller brain size.
604 The position of the orbitotemporal canal of *M. crusafonti* (Fig. 7C) is similar to
605 that of the late Oligocene sciurid *Pr.* cf. *rachelae* (Fig. 8D) in being near the ventral extent
606 of the temporal lobe. This structure is positioned more ventrally in *M. crusafonti*
607 compared to ischyromyid rodents and the early Oligocene sciurid *C. wilsoni* (Figs 8C, E;
608 Bertrand *et al.* 2017, 2019*b*). A ventrally positioned canal reflects a ventral expansion of
609 the neocortex, based on the inferred relationship between the canal and the rhinal fissure
610 in sciurids (Bertrand *et al.* 2017). In extant squirrels the orbitotemporal canal is even more
611 ventrally positioned than in *Pr.* cf. *rachelae* (e.g., Fig. 8A–B), thus resulting in a greater
612 neocortical surface area. This canal is straight in *M. crusafonti* and morphologically
613 similar to that of the flying squirrels *A. tephromelas* and *Pe. petaurista* (Bertrand *et al.*
614 2017). The neocortex of *M. crusafonti* represents 30.2 % of the total endocast surface

615 area, which is in the range of the values obtained for other extinct squirrels (Fig. 9C, Table
616 3; Grau-Camats *et al.* 2021, table S4). In extant squirrels the ratio is higher, ranging from
617 33.8 % to 39.3 % and for flying squirrels specifically, the range of values is between 33.8
618 % and 36.7 % (Fig. 9C, Table 3; Bertrand *et al.* 2017; Grau-Camats *et al.* 2021, table S4).
619 This result contrasts with ischyromyids, which range from 16.3 % to 23 % (Bertrand *et*
620 *al.* 2016*b*, 2018, 2019*b*). Log-transformed neocortical surface area shows a positive and
621 highly significant correlation with log-transformed endocranial surface area, the latter
622 variable explaining a significant part of existing variance (r^2>0.90; Table 4). Our analyses
623 show that phylogenetic signal is strong (λ>1; see Table 4), which would suggest that more
624 closely related species display more similar neocortical sizes in our sample (Fig. 9D).
625 However, this result appears to be mainly driven by ischyromyid rodents as they have a
626 much lower neocortical surface area percentage compared to extinct and extant squirrels.
627 Indeed, after rerunning the PGLS analysis without Ischyromyidae, λ dropped close to 0
628 (and correlation increased to r^2>0.99; Table 4), suggesting that the impact of phylogeny
629 on the relative size of the neocortex is not strong among extinct and extant squirrels.
630 Nevertheless, the neocortical surface area in *M. crusafonti* is slightly smaller than would
631 be expected for its endocranial surface area (Fig. 9D). *Miopetaurista crusafonti* has
632 residual values from the regression line that are close to those calculated for other fossil
633 squirrels, *Pr.* cf. *rachelae* and *C. wilsoni* (Fig. 9D, Bertrand *et al.* 2017, 2018; Grau-
634 Camats *et al.* 2021, tables S6–S7).

635 The hypophyseal fossa is poorly defined, although there is a slight bulge in the
636 endocast just posterior to the optic chiasm that might mark its position. A poorly
637 demarcated fossa is also characteristic of *C. wilsoni* (Fig. 8C) and most extant sciurids
638 studied here, although it is more salient in some ischyromyids (e.g., Fig. 8E; Bertrand *et*
639 *al.* 2016*b*, 2017, 2018, 2019*b*; Bertrand & Silcox 2016).

Cerebellum. The caudal region of the endocast of *M. crusafonti* is damaged. The vermis of the cerebellum is visible, separated from the left lateral lobe of the cerebellum by the paramedian fissure (Fig. 7A, C; Appendix S1). Only the left petrosal lobe (=paraflocculus, see Bertrand *et al.* 2020) is preserved, therefore, the volume calculated for the left petrosal lobe was compared to the volume for the left side of the endocast (Table 3; Grau-Camats *et al.* 2021, table S4). *Miopetaurista crusafonti* has relatively smaller petrosal lobules (1.9 % of total endocast volume) compared to the other fossil squirrels, *C. wilsoni* (3.2 %) and *Pr.* cf. *rachelae* (3.3 %), thus being in the range of extant squirrels (0.9 %–2.3 %) and in the upper part of the range of ischyromyid rodents (0.4 %–2.1 %; Bertrand *et al.* 2017, 2018, 2019*b*). Compared to extant pteromyins, *M. crusafonti* is in the upper range of variation for the petrosal lobule volume ratio (0.9 %–1.7 %). Log-transformed petrosal lobule volume shows a positive and highly significant correlation with both log-transformed endocranial volume and body mass. Both endocranial volume and body mass explain a low proportion of the existing variance (r^2 <0.60; Table 4). Furthermore, the phylogenetic signal is low (λ~0.3; see Table 4) suggesting that closely related species are less likely to exhibit similar relative and absolute petrosal lobule sizes and that other factors may affect the size of this brain structure. The size of the petrosal lobules of *M. crusafonti* is equivalent to the value expected for its endocranial volume compared to modern sciurids (Fig. 9E). Four extant flying squirrels are below the regression line while the remaining three (i.e., *Pe. petaurista*, *A. tephromelas* and *M. crusafonti*) are above it. This relationship is nearly identical when looking at the relationship between petrosal lobule size and body mass; however, in this instance, *M. crusafonti* lies slightly closer to *Pe. petaurista* and well above the regression line (Fig. 9F). It is worth noting that one extant flying squirrel (*Petinomys setosus*) in our dataset lacks the subarcuate fossa entirely (Table 3; Grau-

Camats *et al.* 2021, table S4) and therefore has no petrosal lobules on the endocast (Bertrand *et al.* 2017).

Cranial nerves and blood vessels. The ventral region of the endocast is damaged, particularly on its posterior half, but several cranial nerves can be observed (Fig. 7B, Appendix S1). Casts of both optic nerves and the optic chiasm are partly preserved in *M. crusafonti*, with the chiasm being located just anterior to the point at which the oculomotor nerve would have left the brain. Its location is difficult to identify as this area of the cranium is not well-preserved; however, the chiasm appears to be located dorsal to the posterior nasal spine (Fig. 7B). The sphenorbital fissure is not preserved. Casts of the buccinator and masseteric nerves (branches of nerve V_3) are partly preserved on both sides and exit through the masticatory foramen, which demonstrates that they would have had a course separate from the other parts of V_3 exiting through the foramen ovale (Fig. 7). The casts of mandibular (V_3), facial (VII) and vestibulocochlear (VIII) nerves are observable on the left side of the endocast only. The position of the different casts of the nerves resembles the closely-related *Pe. petaurista* (Fig. 8A). The superior sagittal sinus is demarcated (Fig. 7A), being similar in morphology to *C. wilsoni, Pr.* cf. *rachelae* (Fig. 8C–D) and most modern sciurids in our comparative sample (see Bertrand *et al.* 2017, 2018). It differs from the condition observed in ischyromyid rodents, in which the superior sagittal sinus is less well marked (e.g., Bertrand *et al.* 2019*b*). The transverse and sigmoid sinuses are visible on the left side of the endocast of *M. crusafonti* (Fig. 7C), but the region where the inferior petrosal sinus would have passed is not preserved. The stapedial canal for the distal section of the stapedial artery (Wible & Shelley 2020) can be observed on the ventral region (Fig. 7B–C) and is similarly positioned compared to sciurids and ischyromyids (Bertrand *et al.* 2017, 2018, 2019*b*).

Brain size and encephalization quotient

690 The endocranial volume of *M. crusafonti* (estimated doubling the volume of the
691 most complete side, see Materials and Methods) is 10.82 cm^3. The encephalization
692 quotient (EQ) calculated using the equation by Pilleri *et al.* (1984) is 1.13 (Table 3; Grau-
693 Camats *et al.* 2021, table S5). This value is higher than those calculated for ischyromyids
694 (0.50 to 0.88) and very similar to those for *C. wilsoni* (1.0) and *Pr.* cf. *rachelae* (1.06;
695 Fig. 10A; Bertrand *et al.* 2017, 2018, 2019*b*). *Miopetaurista crusafonti* has an EQ below
696 those of extant Sciurinae, being in the lower range of variation for Callosciurinae (Fig.
697 10A). Log-transformed endocranial volume shows a positive and highly significant
698 correlation with log-transformed body mass, the latter variable explaining great part of
699 the existing variance (r^2=0.89; see Table 4). Phylogenetic signal is relatively low (λ~0.4;
700 see Table 4) implying that closely related species may not necessarily have a similar
701 brain-body mass relationship, suggesting that other factors may impact relative brain size.
702 When assessed against body mass, the endocranial volume of *M. crusafonti* is above the
703 regression line for extant squirrels, below its close relative *Pe. petaurista* (Fig. 10B).

704 **DISCUSSION**

705 Several studies have shown that the encephalization quotient (EQ) increases with
706 time in different mammalian orders (Jerison 1973; Radinsky 1976; Gurche 1982; Silcox
707 *et al.* 2010; Orliac & Gilissen 2012; Yao *et al.* 2012; Bertrand *et al.* 2017, 2018, 2019*b*,
708 2021). On the other hand, a series of papers have shown that EQ also varies as a function
709 of ecology in chiropterans and rodents (Eisenberg & Wilson 1978; Harvey *et al.* 1980;
710 Mace *et al.* 1981; Roth & Thorington 1982; Meier 1983; Pilleri *et al.* 1984; Bertrand *et*
711 *al.* 2017, 2018, 2019*b*). These studies found that arboreality was associated with a higher
712 EQ in rodents, likely because of the requirements of foraging in a complex three-
713 dimensional environment such as found in the treetops. Recently, Bertrand *et al.* (2016*b*,
714 2017, 2018, 2019*b*, 2021) studied the endocasts of ischyromyids and early sciurids

(*Cedromus wilsoni* and *Protosciurus* cf. *rachelae*) as compared to extant aplodontids and sciurids. The Oligocene *C. wilsoni* (subfamily Cedromurinae) and *Pr.* cf. *rachelae* (subfamily Sciurinae, tribe Sciurini), both considered to be scansorial or arboreal squirrels (Korth & Samuels 2015; Bhagat *et al.* 2021), had not yet reached the EQ of their extant relatives. Indeed, *Cedromus* is in the upper part of the range of extant ground squirrels, while *Protosciurus* is in the lower part of the range of tree squirrels. Similarly, the EQ of *M. crusafonti* is 1.07, which is slightly below the range of variation of extant flying squirrels (1.11-1.39; Fig. 10A, Table 3; Grau-Camats *et al.* 2021, table S5), yet there is unquestionable evidence of gliding locomotion in the genus *Miopetaurista* (Casanovas-Vilar *et al.* 2018). Accordingly, the lower EQ suggests that there were temporal trends in this parameter within the sciurid family, as observed in other mammalian families and orders (e.g., Jerison 1973; Radinsky 1976; Silcox *et al.* 2010; Bertrand *et al.* 2019*a*) . In addition, the increase in relative brain size would have occurred independently in the Sciurini and Pteromyini, because early members of both of these Sciurinae tribes (*Protosciurus*, *Miopetaurista*) show lower EQs than extant representatives. Considering that two events of EQ increase occurred in closely related clades, and that the phylogenetic signal is low for the brain-body mass regression, it can be inferred that changes in relative brain size may relate to factors other than phylogeny, such as ecological transitions (Bertrand *et al.* 2017, 2018, 2021).

The comparison of the endocast of *M. crusafonti* to those of extant and extinct sciurids, as well as to the more primitive ischyromyid rodents suggests some significant changes in brain morphology in the flying squirrel lineage. Previous studies have shown that an increase in neocortical surface area ratio occurs in the transition from ischyromyids to sciurids (Bertrand *et al.* 2017, 2018, 2019*a*). The late Oligocene fossil Sciurini *Pr.* cf. *rachelae* and the middle Miocene fossil Pteromyini *M. crusafonti* both

exhibit lower neocortical surface area ratios compared to their respective extant relatives (Fig. 9C; Grau-Camats *et al.* 2021, table S4). Therefore, neocortical surface ratio would have increased independently in tree and flying squirrels, which is the likely cause for the apparent independent increases in EQ discussed above. However, the independent increase in neocortical surface area cannot be solely explained by a possible shift in ecology because all extinct and extant squirrels have larger neocortices than ischyromyid rodents. The gradual increase in neocortical surface area appears to more closely follow a temporal trend than relative brain size and suggests that phylogeny may have more impact on the neocortical size than on overall brain size in our sample. We note that if Ischyromyidae are not included in the estimation of λ for the neocortex, the phylogenetic signal for the relative size of this brain region is markedly lower (Table 4) as all extant squirrels have a higher neocortical surface area compared to extinct squirrels.

Previous studies have shown that an increase in the absolute size of the petrosal lobules occurred in the evolution of the sciurids from ischyromyids as a response to a more arboreal lifestyle in the former group (Bertrand *et al.* 2017, 2018, 2019*b*). Our results show a low phylogenetic signal, thus agreeing with these earlier studies, in that factors other than shared evolutionary story have an important effect on the relative and absolute size of the petrosal lobules. Extant pteromyins of our sample have relatively smaller petrosal lobules compared to sciurins (Fig. 9E; Bertrand *et al.* 2017; Grau-Camats *et al.* 2021, table S4). This difference is already apparent in Miocene taxa. Indeed, while the tree squirrel *Pr.* cf. *rachelae* has relatively large petrosal lobules, the flying squirrel *M. crusafonti* shows a lower relative size, thus resembling its extant relatives (Fig. 9E; Grau-Camats *et al.* 2021, table S4). This suggests a decrease in the relative size of the petrosal lobules in the evolution of flying squirrels which might be related to a packing problem due to the constraints inherent to a skull built to be aerodynamic for gliding (see

765 also Bertrand *et al.* 2021). The functional elements of the petrosal lobules might still be
766 present but in the non-petrosal lobule part of the cerebellum. However, an alternative
767 explanation could be related to a specific adaptation. Tree squirrels spend a considerable
768 amount of time on thin and unstable branches, which implies that balance and control of
769 the head and eye movements are crucial for these animals. In contrast, flying squirrels
770 have a different lifestyle in the trees and to propel themselves in the air, they use more
771 stable and sturdy branches and trunks (Bishop 2006). This suggests that flying squirrels
772 might require less overall eye movement control compared to tree squirrels while
773 navigating the canopy. Pteromyini also have larger auditory bullae compared to tree
774 squirrels (Lu *et al.* 2014). These structures are in contact with the braincase and more
775 specifically with the subarcuate fossa. Using allometric shape deformations, Lu *et al.*
776 (2014) showed that the shape of different cranial regions (e.g., auditory bulla and vault-
777 occiput roundness) changed simultaneously from small to large squirrel specimens.
778 Therefore, enlarged bullae may influence and possibly reduce the space for the petrosal
779 lobules. Alternatively, the auditory bulla may represent a separate module, meaning that
780 the development of both units could be independent. Ultimately, more work will be
781 required to test these hypotheses. The same authors suggested that because the bullae are
782 so large in flying squirrels, hearing might be crucial while gliding. The parietal region of
783 the brain of flying squirrels appears to be more developed, which could potentially
784 suggest enhanced hearing (Bertrand *et al.* 2019*a*). Other studies have indicated that flying
785 squirrels, which are nocturnal gliders, might be using ultrasounds like echolocating bats
786 to ease navigation while gliding (Muul & Alley 1963; but see Chattin 1969). More
787 recently, Murrant *et al.* (2013) identified that flying squirrels were reacting to their own
788 high-frequency vocalizations and therefore were capable to hear ultrasonic sounds. The
789 use of echolocation in flying squirrels is debated and has just begun to be studied in detail,

790 but there is no direct evidence of echo-based navigation so far (Newar & Bowman 2020).
791 Flying squirrels have large eyes and undoubtedly use visual cues during glides, but they
792 may be also assisted by the use of ultrasound (Murrant *et al.* 2013). Therefore, the
793 observed decrease in the size of the petrosal lobules could result from an accommodation
794 for other biological needs such as hearing. More work is required to better understand the
795 relationship between the neurosensory system of flying squirrels and how they navigate
796 through the canopy.

797 Finally, previous studies have shown that a decrease in the size of the olfactory
798 bulbs occurred through time from ischyromyids to sciurids (Bertrand *et al.* 2017, 2018,
799 2019*b*). The relative size of the olfactory bulbs in *M. crusafonti* is slightly below the range
800 of to those of other members of the subtribe Pteromyina (i.e., large flying squirrel clade),
801 including the closely related *Pe. petaurista*, while that of the sciurin *Pr.* cf. *rachelae* is
802 conspicuously in the upper range of the extant tree squirrels variation (Grau-Camats *et al.*
803 2021, table S4). Interestingly, *Glaucomys volans*, *Hylopetes spadiceus* and *Petinomys*
804 *setosus*, the studied members of the subtribe Glaucomyina (i.e., small flying squirrel
805 clade), all show relatively larger olfactory bulbs, in the range of other extant squirrel
806 groups (see Grau-Camats *et al.* 2021, table S4). This could suggest that a decrease in the
807 relative size of the olfactory bulbs occurred after the Pteromyina/Glaucomyina split.
808 Despite exhibiting a relatively small neocortex, closer to the condition in other Oligocene
809 squirrels rather than to extant species, *M. crusafonti* already exhibits features
810 characteristic of Pteromyini (and more specifically the Pteromyina) such as low petrosal
811 lobule and olfactory bulb volume ratios.

812 **CONCLUSIONS**

813 Squirrels are generally regarded as an anatomically conservative group and flying
814 squirrels are no exception, the oldest skeleton of a flying squirrel, belonging to

Miopetaurista neogrivensis and dating back to 11.6 Ma, being very similar in many aspects of morphology to the extant giant flying squirrel *Petaurista* (Casanovas-Vilar *et al.* 2018). The crania of both *M. neogrivensis* and the closely-related *Miopetaurista crusafonti* described here are also remarkably similar to those of *Petaurista* and other large flying squirrels (subtribe Pteromyina) such as *Aeromys* and *Biswamoyopterus*, differing only in cheek tooth morphology and a few minor details in the cranium, such as the morphology of the temporal ridges. Endocranial morphology, as well as the relative volume of the different brain regions are very similar to other Pteromyina, showing for example the relatively reduced petrosal lobules characteristic of flying squirrels in comparison to other extant squirrels. However, the encephalization quotient (EQ) of *M. crusafonti* is slightly below that of extant flying squirrels. A temporal trend in EQ increase has been previously reported for sciurids and other mammal families (Jerison 1973; Radinsky 1976; Gurche 1982; Silcox *et al.* 2010; Orliac & Gilissen 2012; Yao *et al.* 2012; Bertrand *et al.* 2017, 2018, 2019*b*), but this parameter has also been shown to vary with locomotor mode, arboreal and gliding rodent species showing higher values than terrestrial ones (Bertrand *et al.* 2021). Since *Miopetaurista* was certainly a glider, like its extant relatives, the conspicuously lower EQ must be attributed to its older age rather than to different locomotion. Even though this should be tested in additional squirrel groups, these results support an independent temporal increase in EQ in different squirrel clades, further showing that, in terms of relative brain size, flying squirrels are not so conservative.

Author contributions. MGC, OCB, MTS and ICV contributed to the conception and design of the study. JP acquired the CT data, MGC, OCB, SLT segmented the specimens and acquired quantitative measurements. MGC and OCB carried out the statistical

analyses. MGC and OCB drafted the article with important contributions by all other authors. All authors gave final approval before submission.

Acknowledgements. This publication is part of project I+D+i PID2020-117289GBI00 funded by MCIN/AEI/10.13039/501100011033/. It has also been supported by the Spanish Agencia Estatal de Investigación and European Regional Development Fund of the European Union (CGL2016-76431-P and CGL2017-82654-P); the Generalitat de Catalunya (CERCA Programme); a Marie Skłodowska-Curie Actions: Individual Fellowship (H2020-MSCA-IF-2018-2020; No. 792611) to O.C.B; an NSERC Discovery Grant to M.T.S.; and the Ministerio de Economía y Competitividad (RYC-2013-12470 to I.C.-V.). I.C.-V. is member of the consolidated research group 2017 SGR 116 of the Generalitat de Catalunya. The authors thank Sergio Llácer (ICP) for his help with specimen segmentation, and Sergio Llácer and Javier Serrano (ICP) for preparing the video for Appendix S1. We also thank L. W. Van den Hoek Ostende, S. Van der Mije and P. Kaminga (Naturalis Biodiversity Center, Leiden, the Netherlands) for their assistance during the study of the squirrel collections kept at their institution. We thank S. Thomas for her technical comments and assistance in the preparation of tables and figures. The constructive comments by the two reviewers of this manuscript (J. Maugoust and M.V. Sinitsa) as well as by handling editor (L. Hautier) certainly helped to improve the final result.

DATA ARCHIVING STATEMENT

Data for this study are available in the Dryad Digital Repository: https://doi.org/10.5061/dryad.5qfttdz4pç; 3D surface models of the *Miopetaurista crusafonti* cranium and endocast SNSB 1978 V 1 from Gumpersdorf are available at MorphoSource (www.morphosource.org) with identifier xxxxx.

SUPPORTING INFORMATION

Additional supporting information can be found in the online version of this article.

Appendix S1. Animated rendering of the virtual model of the cranium of *Miopetaurista crusafonti* (SNSB 1978 V 1) from Gumpersdorf (Bavaria) based on μCT data. Main anatomical elements of the cranium and the endocast are indicated.

REFERENCES

ABDUL AZIZ, H., BÖHME, M., ROCHOLL, A., PRIETO, J., WIJBRANS, J. R., BACHTADSE, V. and ULBIG, A. 2010. Integrated stratigraphy and $^{40}Ar/^{39}Ar$ chronology of the early to middle Miocene Upper Freshwater Molasse in western Bavaria (Germany). *International Journal of Earth Sciences*, **99**, 1859–1886.

ASHER, R. J., SMITH, M. R., RANKIN, A. and EMRY, R. J. 2019. Congruence, fossils and the evolutionary tree of rodents and lagomorphs. *Royal Society Open Science*, **6**, 190387.

BALL, S. S. and ROTH, V. L. 1995. Jaw muscles of New World squirrels. *Journal of Morphology*, **224**, 265–291.

BAPST, D. W. 2012. paleotree: an R package for paleontological and phylogenetic analyses of evolution. *Methods in Ecology and Evolution*, **3**, 803–807.

———. 2013. A stochastic rate-calibrated method for time-scaling phylogenies of fossil taxa. *Methods in Ecology and Evolution*, **4**, 724–733.

———. 2014. Preparing paleontological datasets for phylogenetic comparative methods. *In* GARAMSZEGI, L. Z. (ed.) *Modern Phylogenetic Comparative Methods and Their Application in Evolutionary Biology: Concepts and Practice*, Springer, Berlin, Heidelberg, 515–544 pp.

887 BERTRAND, O. C. and SILCOX, M. T. 2016. First virtual endocasts of a fossil rodent:
888 *Ischyromys typus* (Ischyromyidae, Oligocene) and brain evolution in rodents.
889 *Journal of Vertebrate Paleontology*, **36**, e1095762.
890 ———, SCHILLACI, M. A. and SILCOX, M. T. 2016*a*. Cranial dimensions as
891 estimators of body mass and locomotor habits in extant and fossil rodents. *Journal*
892 *of Vertebrate Paleontology*, **36**, e1014905.
893 ———, AMADOR-MUGHAL, F. and SILCOX, M. T. 2016*b*. Virtual endocasts of
894 Eocene *Paramys* (Paramyinae): oldest endocranial record for Rodentia and early
895 brain evolution in Euarchontoglires. *Proceedings of the Royal Society B:*
896 *Biological Sciences*, **283**, 20152316.
897 ———, ——— and ———. 2017. Virtual endocast of the early Oligocene *Cedromus*
898 *wilsoni* (Cedromurinae) and brain evolution in squirrels. *Journal of Anatomy*, **230**,
899 128–151.
900 ———, SAN MARTIN-FLORES, G. and SILCOX, M. T. 2019*a*. Endocranial shape
901 variation in the squirrel-related clade and their fossil relatives using 3D geometric
902 morphometrics: contributions of locomotion and phylogeny to brain shape.
903 *Journal of Zoology*, **308**, 197–211.
904 ———, AMADOR-MUGHAL, F., LANG, M. M. and SILCOX, M. T. 2018. Virtual
905 endocasts of fossil Sciuroidea: brain size reduction in the evolution of fossoriality.
906 *Palaeontology*, **61**, 919–948.
907 ———, ———, ——— and ———. 2019*b*. New virtual endocasts of Eocene
908 Ischyromyidae and their relevance in evaluating neurological changes occurring
909 through time in Rodentia. *Journal of Mammalian Evolution*, **26**, 345–371.

910 ———, PÜSCHEL, H. P., SCHWAB, J. A., SILCOX, M. T. and BRUSATTE, S. L.
911 2021. The impact of locomotion on the brain evolution of squirrels and close
912 relatives. *Communications Biology*, **4**, 460.
913 ———, SHELLEY, S. L., WIBLE, J. R., WILLIAMSON, T. E., HOLBROOK, L. T.,
914 CHESTER, S. G. B., BUTLER, I. B. and BRUSATTE, S. L. 2020. Virtual
915 endocranial and inner ear endocasts of the Paleocene 'condylarth' *Chriacus*: new
916 insight into the neurosensory system and evolution of early placental mammals.
917 *Journal of Anatomy*, **236**, 21–49.
918 BHAGAT, R., BERTRAND, O. C. and SILCOX, M. T. 2021. Evolution of arboreality
919 and fossoriality in squirrels and aplodontid rodents: Insights from the semicircular
920 canals of fossil rodents. *Journal of Anatomy*, **238**, 96–112.
921 BININDA-EMONDS, O. R. P., CARDILLO, M., JONES, K. E., MACPHEE, R. D. E.,
922 BECK, R. M. D., GRENYER, R., PRICE, S. A., VOS, R. A., GITTLEMAN, J.
923 L. and PURVIS, A. 2007. The delayed rise of present-day mammals. *Nature*, **446**,
924 507–512.
925 BISHOP, K. L. 2006. The relationship between 3-D kinematics and gliding performance
926 in the southern flying squirrel, *Glaucomys volans*. *Journal of Experimental*
927 *Biology*, **209**, 689–701.
928 BRAUER, K. and SCHOBER, W. 1970. *Katalog der Säugetiergehirne. Catalogue of*
929 *mammalian brains*. VEB Gustav Fischer, Jena, Germany.
930 DE BRUIJN, H. 1999. Superfamily Sciuroidea. *In* RÖSSNER, G. E. and HEISSIG, K.
931 (eds.) *The Miocene Land Mammals of Europe*, Verlag Dr. Friedrich Pfiel, Munich,
932 271–280 pp.
933 CASANOVAS-VILAR, I., ALMÉCIJA, S. and ALBA, D. M. 2015. Late Miocene flying
934 squirrels from Can Llobateres 1 (Vallès-Penedès Basin, Catalonia): systematics

and palaeobiogeography. *Palaeobiodiversity and Palaeoenvironments*, **95**, 353–372.

———, GARCIA-PORTA, J., FORTUNY, J., SANISIDRO, Ó., PRIETO, J., QUEREJETA, M., LLÁCER, S., ROBLES, J. M., BERNARDINI, F. and ALBA, D. M. 2018. Oldest skeleton of a fossil flying squirrel casts new light on the phylogeny of the group. *ELife*, **7**, e39270.

CHATTIN, D. 1969. Acoustical echolocation in flying squirrels.BA Thesis, Reed College, Portland, 76pp.

DAAMS, R. 1977. Aragonian sciuroptera (Sciuridae, Rodentia, Mammalia) from Spain. *Proceedings of the Koninklijke Nederlandse Akademie van Wetenschappen*, **80(5)**, 356–359.

DAXNER-HÖCK, G. and MEIN, P. 1975. Taxonomische Probleme um das Genus *Miopetaurista* Kretzoi, 1962 (Fam. Sciuridae). *Paläontologische Zeitschrift*, **49**, 75–77.

DAXNER-HÖCK, G. and HÖCK, E. 2015. *Catalogus Fossilium Austriae. Ein systematisches Verzeichnis aller auf österreichsichem Gebiet festgestellten Fossilien. Band 4. Rodentia neogenica*. *Catalogus Fossilium Austriae. Ein Systematisches Verzeichnis Aller Auf Österreichsichem Gebiet Festgestellten Fossilien.* Verlag der Österreichischen Akademie der Wissenschaften.

EISENBERG, J. F. and WILSON, D. E. 1978. Relative brain size and feeding strategies in the Chiroptera. *Evolution*, **32**, 740–751.

EMRY, R. J. and KORTH, W. W. 2007. A new genus of squirrel (Rodentia, Sciuridae) from the mid-Cenozoic of North America. *Journal of Vertebrate Paleontology*, **27**, 693–698.

FABRE, P.-H., HAUTIER, L., DIMITROV, D. and DOUZERY, E. J. P. 2012. A glimpse on the pattern of rodent diversification: a phylogenetic approach. *BMC Evolutionary Biology*, **12**, 88.

FAHLBUSCH, V. 1979. Flughörnchen-Schädel (*Miopetaurista crusafonti*; Inv.-Nr. 1978 V1). **7**, 18–19.

FRANZEN, J. L. and STORCH, G. 1975. Die unterpliozäne (turolische) Wirbeltierfauna von Dorn-Dürkheim, Rheinhessen (SW-Deutschland). 1. Entdeckung, Geologie, Mammalia: Carnivora, Proboscidea, Rodentia. Grabungsergebnisse 1972-1973. *Senckenbergiana Lethaea*, **56**, 233–303.

FRANZEN, J. L., PICKFORD, M. and COSTEUR, L. 2013. Palaeobiodiversity, palaeoecology, palaeobiogeography and biochronology of Dorn-Dürkheim 1—a summary. *Palaeobiodiversity and Palaeoenvironments*, **93**, 277–284.

GRAFEN, A. and HAMILTON, W. D. 1989. The phylogenetic regression. *Philosophical Transactions of the Royal Society of London. B, Biological Sciences*, **326**, 119–157.

GRAU-CAMATS, M., BERTRAND, O. C., PRIETO, J., LÓPEZ-TORRES, S., SILCOX, M. T. and CASANOVAS-VILAR, I. 2021. Data from: A *Miopetaurista* (Sciuridae, Rodentia) cranium from the middle Miocene of Bavaria (Germany) and brain evolution in flying squirrels. *Dryad Digital Repository*.

GREGOR, H.-J. 1982. *Die jungtertiären Floren Süddeutschlands. Paläokarpologie, Phytostratigraphie, Paläoökologie, Paläoklimatologie*. Ferdinand Enke, Stuttgart.

GURCHE, J. A. 1982. Early primate brain evolution. *In* ARMSTRONG, E. and FALK, D. (eds.) *Primate Brain Evolution: Methods and Concepts*, Springer US, Boston, MA, 227–246 pp.

HAN, G., MAO, F., BI, S., WANG, Y. and MENG, J. 2017. A Jurassic gliding euharamiyidan mammal with an ear of five auditory bones. *Nature*, nature24483.

HARVEY, P. H., CLUTTON-BROCK, T. H. and MACE, G. M. 1980. Brain size and ecology in small mammals and primates. *Proceedings of the National Academy of Sciences*, **77**, 4387–4389.

HERRON, M. D., CASTOE, T. A. and PARKINSON, C. L. 2004. Sciurid phylogeny and the paraphyly of Holarctic ground squirrels (*Spermophilus*). *Molecular Phylogenetics and Evolution*, **31**, 1015–1030.

HILGEN, F. J., LOURENS, L. J. and VAN DAM, J. A. 2012. The Neogene Period. *In* GRADSTEIN, F. M., OGG, J. G., SCHMITZ, M. and OGG, G. (eds.) *The Geologic Time Scale 2012*, Elsevier, Amsterdam, 923–978 pp.

HUELSENBECK, J. P. and RONQUIST, F. 2001. MRBAYES: Bayesian inference of phylogenetic trees. *Bioinformatics*, **17**, 754–755.

IVES, A. R. 2019. R2s for correlated data: phylogenetic models, LMMs, and GLMMs. *Systematic Biology*, **68**, 234–251.

JACKSON, S. 2012. *Gliding Mammals of the World*. CSIRO Publishing, Collingwood, Vic.

JACKSON, S. M. and THORINGTON, R. W. Jr. 2012. *Gliding Mammals: Taxonomy of Living and Extinct Species*. *Smithsonian Contributions to Zoology*. Smithsonian Institution Scholarly Press, Washington DC.

JERISON, H. J. 1973. *Evolution of the Brain and Intelligence*. Academic Press, New York, NY.

———. 2012. Digitized fossil brains: neocorticalization. *Biolinguistics*, **6**, 383–392.

KIRSCHER, U., PRIETO, J., BACHTADSE, V., AZIZ, H. A., DOPPLER, G., HAGMAIER, M. and BÖHME, M. 2016. A biochronologic tie-point for the base

of the Tortonian stage in European terrestrial settings: Magnetostratigraphy of the topmost Upper Freshwater Molasse sediments of the North Alpine Foreland Basin in Bavaria (Germany). *Newsletters on Stratigraphy*, **49**, 445–467.

KORTH, W. W. 1994. *The Tertiary Record of Rodents in North America*. Plenum Press.

——— and EMRY, R. J. 1991. The skull of *Cedromus* and a review of the Cedromurinae (Rodentia, Sciuridae). *Journal of Paleontology*, **65**, 984–994.

——— and SAMUELS, J. X. 2015. New rodent material from the John Day Formation (Arikareean, Middle Oligocene to Early Miocene) of Oregon. *Annals of Carnegie Museum*, **83**, 19–84.

LI, Q., LI, X.-Y., JACKSON, S. M., LI, F., JIANG, M., ZHAO, W., SONG, W.-Y. and JIANG, X.-L. 2019. Discovery and description of a mysterious Asian flying squirrel (Rodentia, Sciuridae, *Biswamoyopterus*) from Mount Gaoligong, southwest China. *ZooKeys*, **864**, 147–160.

LONG, A., BLOCH, J. I. and SILCOX, M. T. 2015. Quantification of neocortical ratios in stem primates. *American Journal of Physical Anthropology*, **157**, 363–373.

LU, X., GE, D., XIA, L., HUANG, C. and YANG, Q. 2014. Geometric morphometric study of the skull shape diversification in Sciuridae (Mammalia, Rodentia). *Integrative Zoology*, **9**, 231–245.

LUO, Z.-X., MENG, Q.-J., GROSSNICKLE, D. M., LIU, D., NEANDER, A. I., ZHANG, Y.-G. and JI, Q. 2017. New evidence for mammaliaform ear evolution and feeding adaptation in a Jurassic ecosystem. *Nature*, **548**, 326–329.

MACE, G. M., HARVEY, P. H. and CLUTTON-BROCK, T. H. 1981. Brain size and ecology in small mammals. *Journal of Zoology*, **193**, 333–354.

MACRINI, T. E., ROUGIER, G. W. and ROWE, T. 2007. Description of a cranial endocast from the fossil mammal *Vincelestes neuquenianus* (Theriiformes) and

its relevance to the evolution of endocranial characters in therians. *The Anatomical Record*, **290**, 875–892.

MARTIN, R. D. 1990. Evolution of the primate central nervous system. *In Primate Origins and Evolution: A Phylogenetic Reconstruction*, Princeton University Press, Princeton, New Jersey, 357–426 pp.

MAYR, H. 1979. Gebissmorphologische Untersuchungen an miozänen Gliriden Mammalia, Rodentia Süddeutschlands.PhD Dissertation, Ludwig-Maximillians-Universität München, Munich, 380pp.

MCKENNA, M. C. and BELL, S. K. 1997. *Classification of Mammals*. Columbia University Press, New York.

MEIER, P. T. 1983. Relative brain size within the North American Sciuridae. *Journal of Mammalogy*, **64**, 642–647.

MEIN, P. 1970. Les sciuroptères (Mammalia, Rodentia) néogènes d'Europe Occidentale. *Geobios*, **3**, 7–77.

MEIN, P. and ROMAGGI, J.-P. 1991. Un gliridé (mammalia, rodentia) planeur dans le miocène supérieur de l'Ardèche: Une adaptation non retrouvée dans la nature actuelle. *Geobios*, **24**, 45–50.

MENG, J., HU, Y. and LI, C. 2003. The osteology of *Rhombomylus* (Mammalia, Glires): implications for phylogeny and evolution of Glires. *Bulletin of the American Museum of Natural History*, **275**, 1–247.

———, ———, WANG, Y., WANG, X. and LI, C. 2006. A Mesozoic gliding mammal from northeastern China. *Nature*, **444**, 889–893.

MERCER, J. M. and ROTH, V. L. 2003. The effects of Cenozoic global change on squirrel phylogeny. *Science*, **299**, 1568–1572.

MURPHY, W. J., FOLEY, N. M., BREDEMEYER, K. R., GATESY, J. and SPRINGER, M. S. 2021. Phylogenomics and the genetic architecture of the placental mammal radiation. *Annual Review of Animal Biosciences*, **9**, 29–53.

MURRANT, M. N., BOWMAN, J., GARROWAY, C. J., PRINZEN, B., MAYBERRY, H. and FAURE, P. A. 2013. Ultrasonic vocalizations emitted by flying squirrels. *PLoS ONE*, **8**, e73045.

MUUL, I. and ALLEY, J. W. 1963. Night gliders of the woodlands: vociferous *Glaucomys* rarely appears. *Natural History Magazine*, 18–25.

NEWAR, S. L. and BOWMAN, J. 2020. Think before they squeak: Vocalizations of the squirrel family. *Frontiers in Ecology and Evolution*, **8**, 193.

NICOLAS, V., WENDELEN, W., BARRIERE, P., DUDU, A. and COLYN, M. 2008. Morphometric variation in *Hylomyscus alleni* and *H. stella* (Rodentia: Muridae), and description of a new species. *Journal of Mammalogy*, **89**, 222–231.

O'LEARY, M. A., BLOCH, J. I., FLYNN, J. J., GAUDIN, T. J., GIALLOMBARDO, A., GIANNINI, N. P., GOLDBERG, S. L., KRAATZ, B. P., LUO, Z.-X., MENG, J., NI, X., NOVACEK, M. J., PERINI, F. A., RANDALL, Z. S., ROUGIER, G. W., SARGIS, E. J., SILCOX, M. T., SIMMONS, N. B., SPAULDING, M., VELAZCO, P. M., WEKSLER, M., WIBLE, J. R. and CIRRANELLO, A. L. 2013. The Placental Mammal Ancestor and the Post–K-Pg Radiation of Placentals. *Science*, **339**, 662–667.

ORLIAC, M. J. and GILISSEN, E. 2012. Virtual endocranial cast of earliest Eocene *Diacodexis* (Artiodactyla, Mammalia) and morphological diversity of early artiodactyl brains. *Proceedings of the Royal Society B: Biological Sciences*, **279**, 3670–3677.

PAGEL, M. 1999. Inferring the historical patterns of biological evolution. *Nature*, **401**, 877–884.

PILLERI, G., GIHR, M. and KRAUS, C. 1984. Cephalization in rodents with particular reference to the Canadian beaver (*Castor canadensis*). *In* PILLERI, G. (ed.) *Investigations on Beavers*, Brain Anatomy Institute, Berne, 11–102 pp.

PINHEIRO, J., BATES, D., DEBROY, S., SARKAR, D. and R CORE TEAM. 2020. *Nlme: Linear and Nonlinear Mixed Effects Models*. *R Package*. .

PRIETO, J. and RUMMEL, M. 2016. Some considerations on small mammal evolution in Southern Germany, with emphasis on Late Burdigalian-Earliest Tortonian (Miocene) cricetid rodents. *Comptes Rendus Palevol*, **15**, 837–854.

R CORE TEAM. 2020. *R: A language and environment for statistical computing*. R Foundation for Statistical Computing, Vienna.

RADINSKY, L. 1976. Oldest horse brains: more advanced than previously realized. *Science*, **194**, 626–627.

RONQUIST, F. and HUELSENBECK, J. P. 2003. MrBayes 3: Bayesian phylogenetic inference under mixed models. *Bioinformatics*, **19**, 1572–1574.

ROTH, V. L. and THORINGTON, R. W. Jr. 1982. Relative brain size among African squirrels. *Journal of Mammalogy*, **63**, 168–173.

SILCOX, M. T., BENHAM, A. E. and BLOCH, J. I. 2010. Endocasts of *Microsyops* (Microsyopidae, Primates) and the evolution of the brain in primitive primates. *Journal of Human Evolution*, **58**, 505–521.

SIMPSON, G. G. 1945. The principles of classification and a classification of mammals. *Bulletin of the American Museum of Natural History*, **85**, 1–350.

SINITSA, M. V., POGODINA, N. V. and KRYUCHKOVA, L. Y. 2019. The skull of *Spermophilus nogaici* (Rodentia: Sciuridae: Xerinae) and the affinities of the

earliest Old World ground squirrels. *Zoological Journal of the Linnean Society*, **186**, 826–864.

SPRINGER, M. S., MURPHY, W. J., EIZIRIK, E. and O'BRIEN, S. J. 2003. Placental mammal diversification and the Cretaceous–Tertiary boundary. *Proceedings of the National Academy of Sciences*, **100**, 1056–1061.

STEPPAN, S. J., STORZ, B. L. and HOFFMANN, R. S. 2004. Nuclear DNA phylogeny of the squirrels (Mammalia: Rodentia) and the evolution of arboreality from c-myc and RAG1. *Molecular Phylogenetics and Evolution*, **30**, 703–719.

STORCH, G., ENGESSER, B. and WUTTKE, M. 1996. Oldest fossil record of gliding in rodents. *Nature*, **379**, 439–441.

SYMONDS, M. R. E. and BLOMBERG, S. P. 2014. A Primer on Phylogenetic Generalised Least Squares. *In* GARAMSZEGI, L. Z. (ed.) *Modern Phylogenetic Comparative Methods and Their Application in Evolutionary Biology: Concepts and Practice*, Springer, Berlin, Heidelberg, 105–130 pp.

THORINGTON, R. W., Jr. 1984. Flying squirrels are monophyletic. *Science*, **225**, 1048–1050.

——— and DARROW, K. 2000. Anatomy of the squirrel wrist: bones, ligaments and muscles. *Journal of Morphology*, **246**, 85–102.

———, PITASSY, D. and JANSA, S. A. 2002. Phylogenies of flying squirrels (Pteromyinae). *Journal of Mammalian Evolution*, **9**, 99–135.

———, SCHENNUM, C. E., PAPPAS, L. A. and PITASSY, D. 2005. The difficulties of identifying flying squirrels (Sciuridae: Pteromyini) in the fossil record. *Journal of Vertebrate Paleontology*, **25**, 950–961.

WAHLERT, J. H. 1985. Cranial foramina of rodents. *In* LUCKETT, W. P. and HARTENBERGER, J.-L. (eds.) *Evolutionary Relationships among Rodents*, Springer US, Boston, MA, 311–332 pp.

———. 2000. Morphology of the auditory region in *Paramys copei* and other Eocene rodents from North America. *American Museum Novitates*, **3307**, 1–16.

WIBLE, J. R. 1984. The ontogeny and phylogeny of the mammalian cranial arterial pattern.PhD Dissertation, Duke University, Durham, North Carolina, USA, 705pp.

———. 2008. On the cranial osteology of the Hispaniolan solenodon, *Solenodon paradoxus* Brandt, 1833 (Mammalia, Lipotyphla, Solenodontidae). *Annals of Carnegie Museum*, **77**, 321–402.

——— and SHELLEY, S. L. 2020. Anatomy of the petrosal and middle ear of the brown rat, *Rattus norvegicus* (Berkenhout, 1769) (Rodentia, Muridae). *Annals of Carnegie Museum*, **86**, 1–35.

YAO, L., BROWN, J.-P., STAMPANONI, M., MARONE, F., ISLER, K. and MARTIN, R. D. 2012. Evolutionary change in the brain size of bats. *Brain, Behavior and Evolution*, **80**, 15–25.

FIGURE CAPTIONS

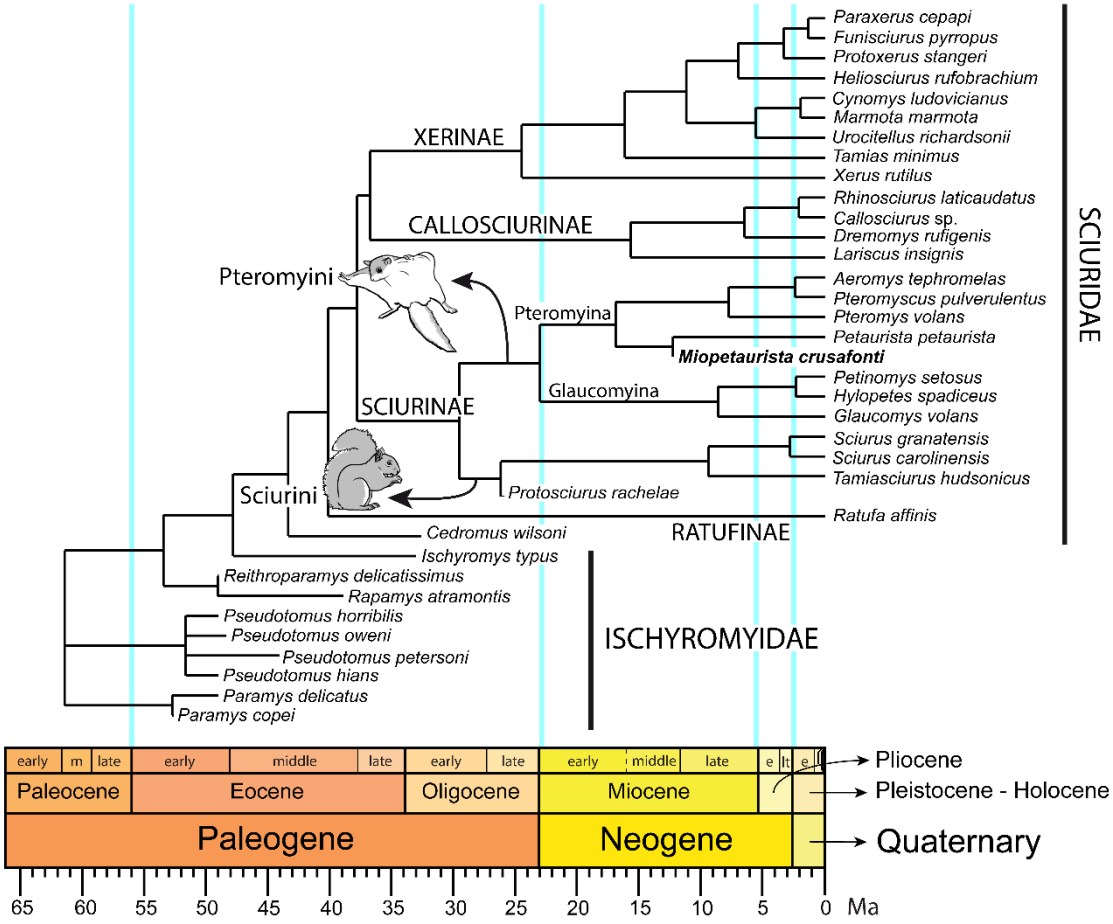

FIG. 1. Phylogenetic relationships and age for Sciuridae and Ischyromyidae discussed in the text. Within the Sciurinae, the flying (Pteromyini) and tree squirrel (Sciurini) clades are highlighted and *Miopetaurista crusafonti* is indicated in bold. Tree topology is mostly based in Korth & Emry (1991), Meng *et al.* (2003) and Casanovas-Vilar *et al.* (2018) (see text for details). This tree is used to perform the Phylogenetic Generalised Least Squares (PGLS) analyses (see text for details).

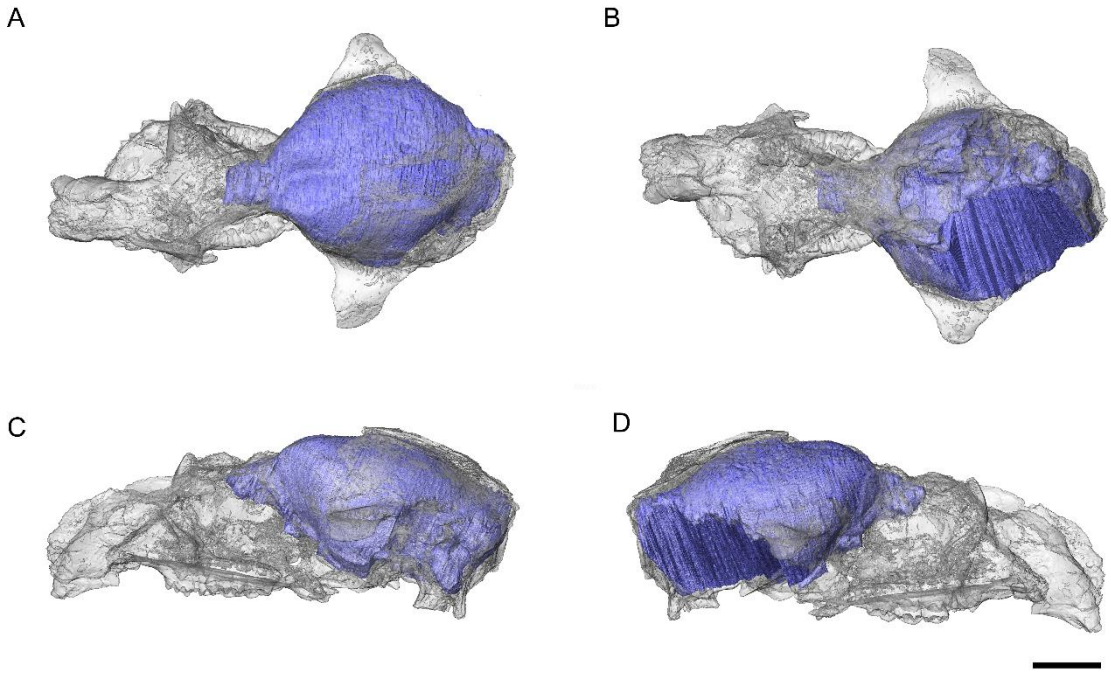

1158

1159 **FIG. 2.** Virtual endocast of *Miopetaurista crusafonti* (SNSB 1978 V 1) inside the
1160 translucent cranium in: A, dorsal; B, ventral; C, left lateral; D, right lateral view. Scale
1161 bar is 10 mm. See Appendix S1 for an animated rendering of the specimen.

1162

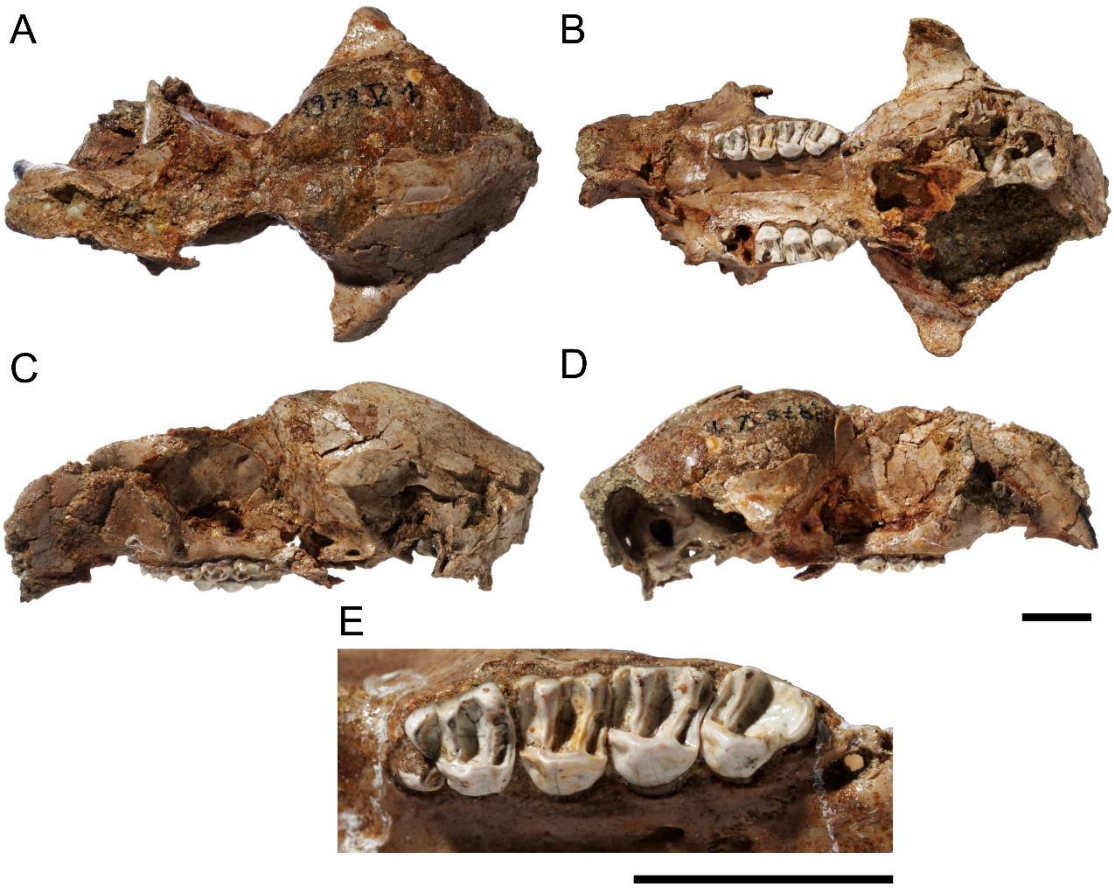

FIG. 3. Cranium of *Miopetaurista crusafonti* (SNSB 1978 V 1) in: A, dorsal; B, ventral; C, left lateral; D, right lateral view. E, detail of the upper left cheek teeth in occlusal view. Scale bar is 10 mm in figures A–D and 5 mm in figure E. Cheek teeth measurements and comparisons are given in Table 1 and Grau-Camats *et al.* (2021, table S1), respectively, while cranial measurements and comparisons are given in Table 2. See Appendix S1 for an animated rendering of the specimen.

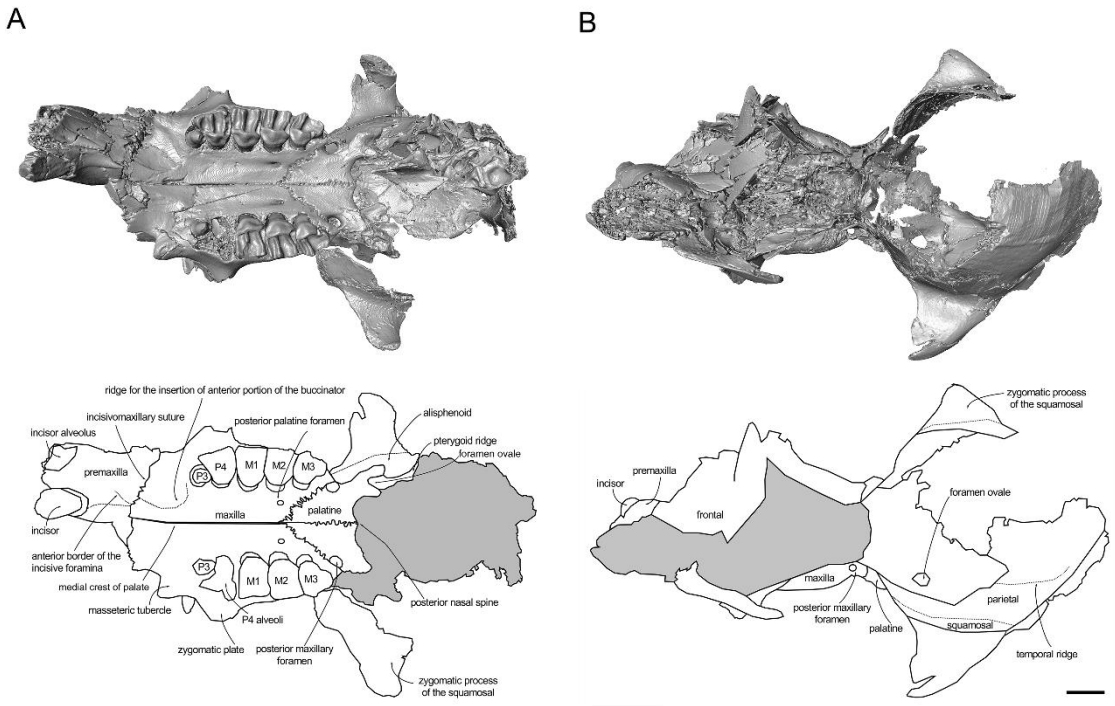

1171

1172 **FIG. 4.** Three-dimensional model of the cranium of *Miopetaurista crusafonti* (SNSB 1978
1173 V 1) based on μCT data and schematic drawing indicating the different anatomical
1174 elements in: A, ventral view; B dorsal view. Gray shading indicates broken areas. Scale
1175 bar is 10 mm. See Appendix S1 for an animated rendering of the specimen.

1176

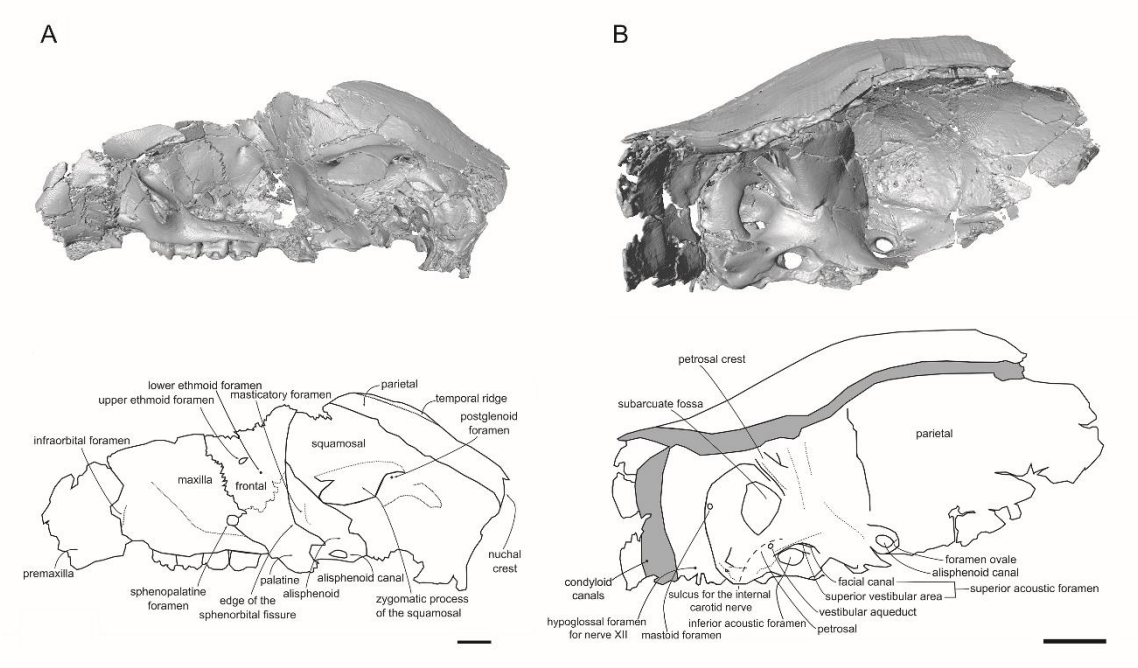

1177

1178 **FIG. 5.** Three-dimensional model of the cranium of *Miopetaurista crusafonti* (SNSB 1978
1179 V 1) based on μCT data and schematic drawing indicating the different anatomical
1180 elements in: A, left lateral view; B, left petrosal in medial view. Gray shading indicates
1181 broken areas. Dashed lines indicate the approximate situation of anatomical features that
1182 cannot be appreciated in this view. Scale bar is 10 mm. See Appendix S1 for an animated
1183 rendering of the specimen.

1184

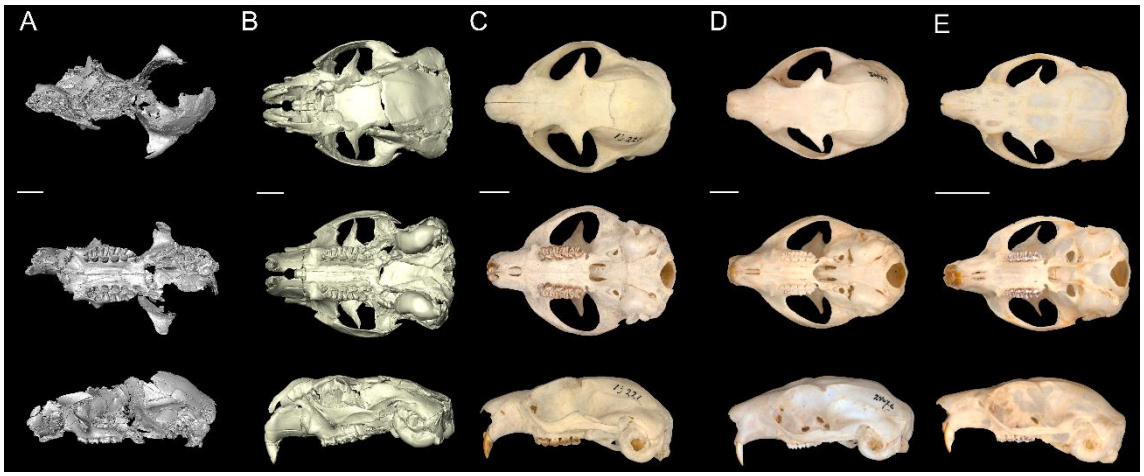

FIG. 6. Crania of extinct and extant flying squirrels in dorsal, ventral and lateral views. A, *Miopetaurista crusafonti* (SNSB 1978 V 1); B, *Miopetaurista neogriviensis* (virtual reconstruction based on IPS56468h and IPS88677); C, *Petaurista petaurista* (ZMA 13418); D, *Aeromys tephromelas* (RMNH 24076); E, *Petinomys sagitta* (RMNH 15512). Scale bars are 10 mm. Cranial measurements and comparisons are given in Table 2.

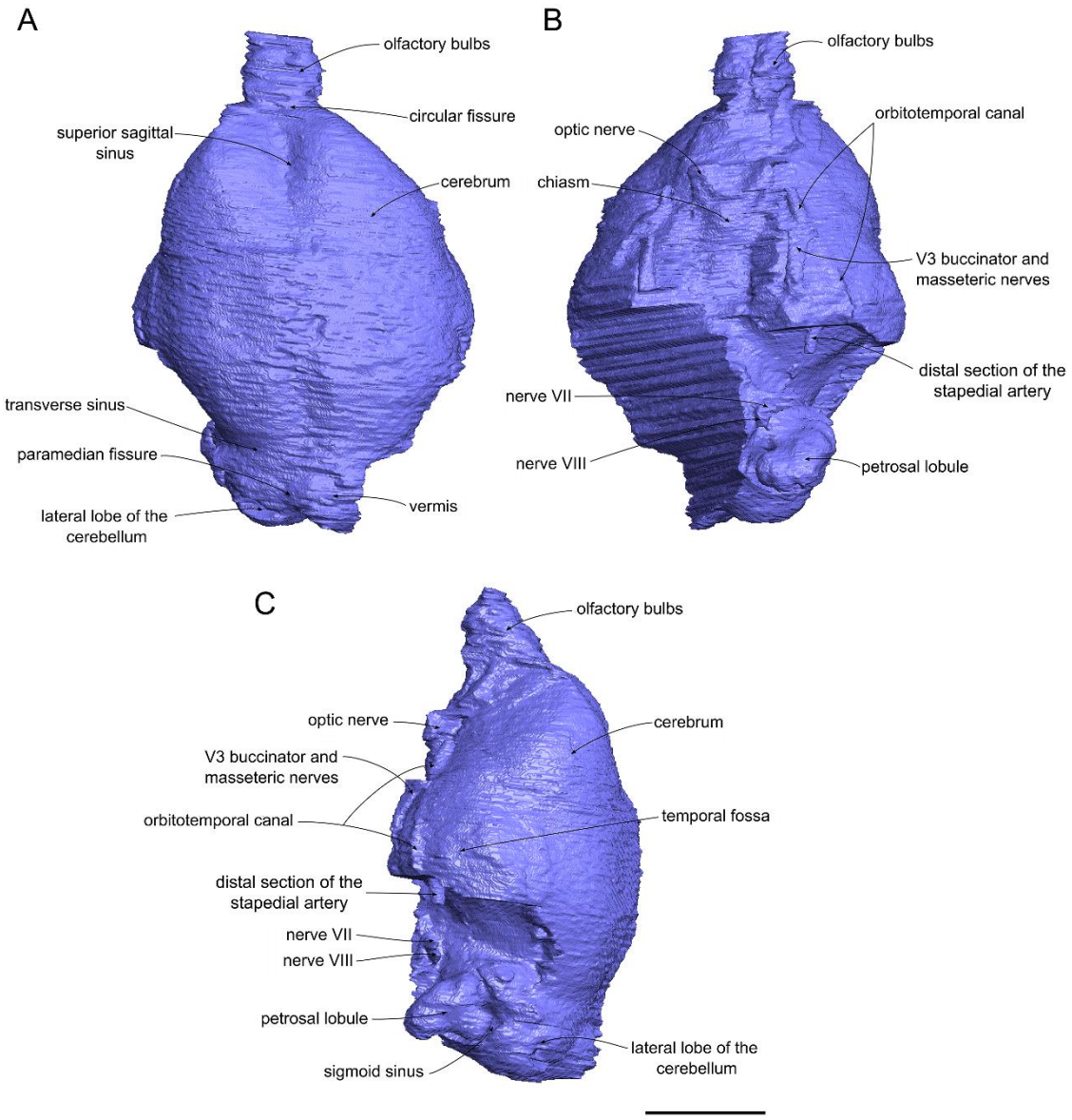

1192

1193 **FIG. 7.** Endocranial morphology of the Miocene fossil flying squirrel *Miopetaurista*
1194 *crusafonti* (SNSB 1978 V 1). Virtual endocast of *M. crusafonti* in: A, dorsal; B, ventral;
1195 C, left lateral view. Scale bar is 10 mm. See Appendix S1 for an animated rendering of
1196 the endocast.

1197

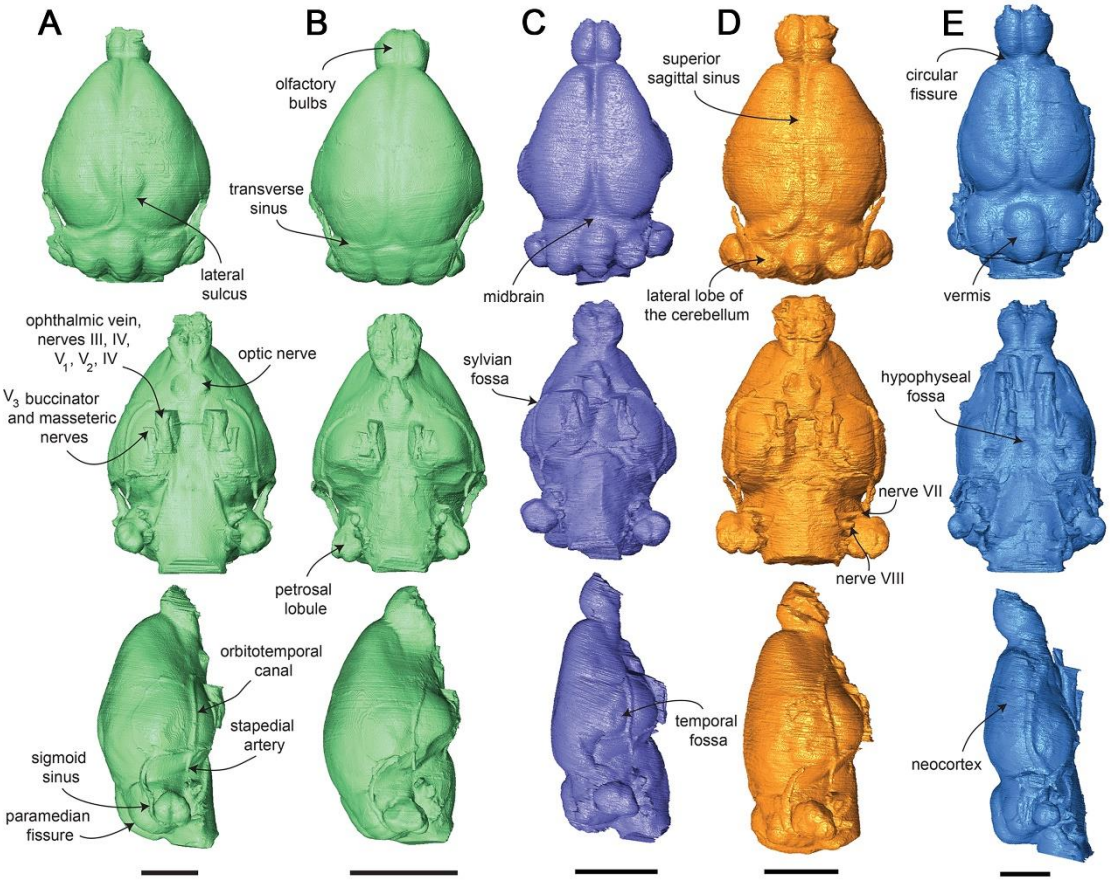

1198

1199 **FIG. 8.** Endocasts of various extinct and extant rodents in dorsal, ventral and right lateral

1200 views. A, *Petaurista petaurista* (USNM 589079); B, *Glaucomys volans* (AMNH

1201 240290); C, *Cedromus wilsoni* (USNM 256584); D, *Protosciurus* cf. *rachelae* (YPM

1202 14737); E, *Paramys delicatus* (AMNH 12506). Scale bars are 10 mm.

1203

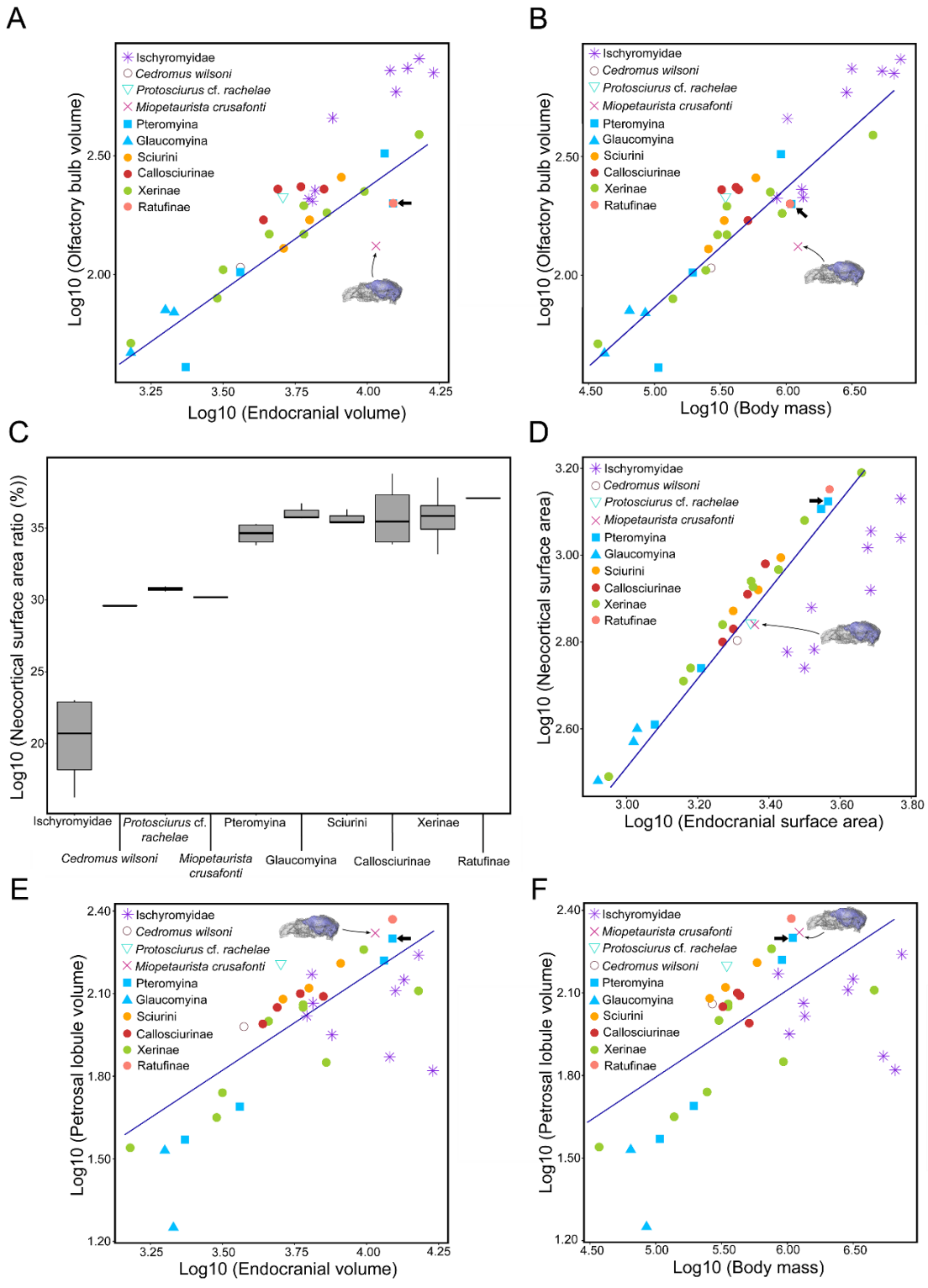

FIG. 9. Bivariate plots and boxplots for endocast measurements in Ischyromyidae and extant and extinct Sciuridae. A, bivariate plot of log 10 (olfactory bulb volume) versus log 10 (endocranial volume); B, bivariate plot of log 10 (olfactory bulb volume) versus log 10 (body mass); C, boxplot of neocortical surface area ratio; D, bivariate plot of log

10 (neocortical surface area) versus log 10 (endocranial surface area); E, bivariate plot of log 10 (petrosal lobule volume) versus log 10 (endocranial volume); F, bivariate plot of log 10 (petrosal lobule volume) versus log 10 (body mass). Phylogenetic generalized least-square (PGLS) regression lines are included for extant Sciuridae. The position of *Miopetaurista crusafonti* SNSB 1978 V 1 from Gumpersdorf as well as that of the extant *Petaurista petaurista* (thick arrow) is indicated in figures (A–B) and (D–F). PGLS regression results are given in Table 4. Residuals associated with the different PGLS regressions are given in Grau-Camats *et al.* (2021, table S6). Body mass, olfactory bulb, petrosal lobule and endocast volume (in mm^3) and neocortical surface area for *Miopetaurista crusafonti* and other extinct and extant sciurid and ischyromyid rodents are given in Grau-Camats *et al.* (2021, table S4).

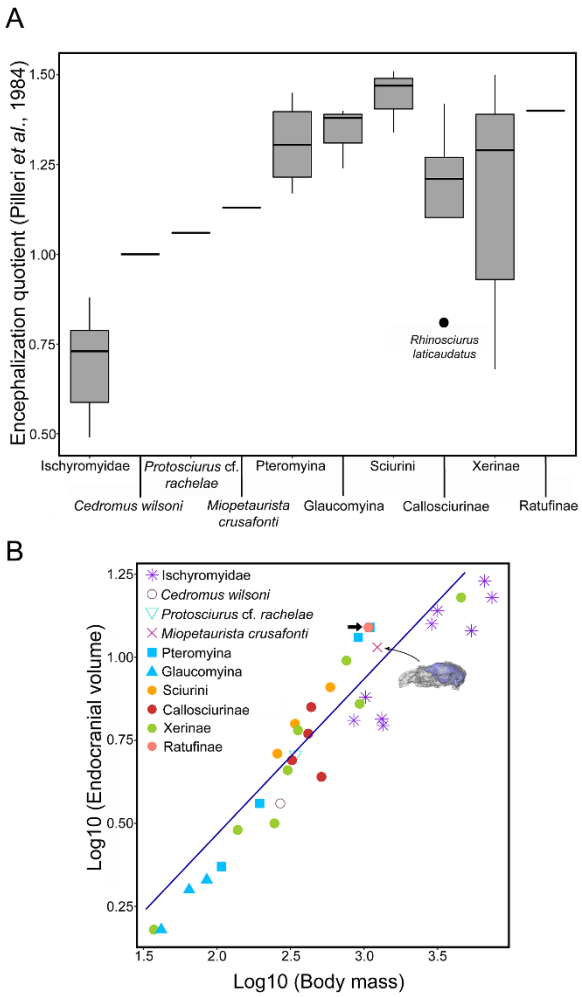

1221

1222 **FIG. 10.** Relationship between endocranial volume and body mass and encephalization
1223 quotients for extinct and extant Sciuridae and Ischyromyidae (see Table 1). A, Boxplot
1224 of EQs based on the equation by Pilleri et al. (1984). B, Bivariate plot of log 10
1225 (endocranial volume) versus log 10 (body mass) for Sciuridae and Ischyromyidae.
1226 Phylogenetic generalised least-square (PGLS) regression line is included for extant
1227 Sciuridae. The position of *Miopetaurista crusafonti* SNSB 1978 V 1 from Gumpersdorf,
1228 as well as that of the extant *Petaurista petaurista* (thick arrow) is indicated in figure B.
1229 PGLS regression results are given in Table 4. Residuals associated with the different
1230 PGLS regressions are given in Grau-Camats *et al.* (2021, table S7). Body mass and
1231 endocast volume (in mm^3) for *Miopetaurista crusafonti* and other extinct and extant
1232 sciurid and ischyromyid rodents are given in Grau-Camats *et al.* (2021, table S4).

TABLE 1. Cheek tooth measurements for *Miopetaurista crusafonti* 1978 V 1 from Gumpersdorf. 'l' stands for left side and 'r' stands for right side. All measurements are in mm.

Element	Length	Width
P3 l	2.49	2.27
P4 l	3.97	4.05
M1 l	3.65	4.51
M2 l	3.72	4.44
M3 l	3.62	3.9
P3 r	2.37	2.16
M1 r	3.54	4.46
M2 r	3.79	4.42
M3 r	3.73	3.99

1238 **TABLE 2.** Cranial measurements for extinct and extant flying squirrels as compared to
1239 *Miopetaurista crusafonti* 1978 V 1 from Gumpersdorf and other extant and extinct flying
1240 squirrels. Cranial measurements for the virtually reconstructed skull of *M. neogrivensis*
1241 are after Casanovas-Vilar *et al.* (2018) . Acronyms and definitions of the measurements
1242 follow Nicolas *et al.* (2008) and Bertrand *et al.* (2016*a*): BNAS, maximum breadth of the
1243 nasals; BRCA, maximum breadth of the braincase; BULL, maximum length of the
1244 auditory bulla; CTL, length of the upper cheek tooth row; DIA, length of the diastema
1245 (from the alveolus of the incisor to the alveolus of the P3); HEBA, henselion–basion
1246 length; HEPA, henselion–palation length; IF, length of the incisive foramen; INTE,
1247 smallest interorbital breadth; LNAS, maximum length of the nasals; PALA, smallest
1248 palatal breadth; RB, maximum rostrum breadth; RH, mediosagittal projection of rostrum
1249 height at the anterior border of the M1; SL, maximum length of the skull. All
1250 measurements are in mm. Estimated measurements (due to breakage or distortion) are
1251 given in parentheses, while '>' indicates that the measurement could not be reliably taken
1252 but certainly exceeded the reported value.

1253

Species and specimen	SL	HEBA	HEPA	IF	DIA	INTE	ZYGO	PALA	CTL	ZYPL	BNAS	LNAS	BULL	BRCA	RH	RB
Miopetaurista crusafonti (1978 V1)	(67.7)	(59.4)	(36.0)	–	>14.7	(9.7)	–	7.3	17.0	8.6	–	–	–	(27.6)	>19.4	>12.1
Miopetaurista neogrivensis (IPS56468h)	(72.4)	(58.6)	(38.8)	6.8	16.1	(20.1)	–	(9.0)	18.4	(8.6)	–	>25.0	19.0	(30.3)	(22.7)	(20.0)
Miopetaurista neogrivensis (IPS88677)	(73.6)	(61.8)	38.1	6.9	17.8	–	(54.6)	(11.2)	17.4	11.3	–	>22.0	(18.9)	(37.2)	(24.1)	(21.7)
Miopetaurista neogrivensis (virtual recons.)	69.8	(58.8)	39.4	6.8	16.4	19.6	46.4	9.5	18.4	10.4	–	>19.2	19.0	37.2	25.1	(23.8)
Petaurista petaurista (ZMA131418)	64.5	54.1	30.7	3.3	12.7	16.7	44.8	7.3	15.5	5.9	12.0	19.4	13.2	29.7	20.2	14.5
Eupetaurus cinereus (19524)	72.3	58.5	35.7	6.2	14.7	18.7	44.1	12.0	19.6	9.0	13.0	24.7	14.7	26.7	23.9	13.8
Aeromys tephromelas (24076)	66.0	53.8	27.6	5.3	15.6	14.2	40.7	8.4	12.3	7.7	11.3	17.2	15.1	31.0	22.0	15.2
Belomys pearsonii (56.046)	43.2	34.3	20.8	2.9	9.3	8.5	26.0	4.8	9.9	4.4	6.4	13.1	10.2	20.1	12.7	8.4
Pteromys volans (40035)	36.5	29.4	15.9	4.3	7.5	9.9	22.6	5.4	6.6	4.6	6.1	11.6	10.5	16.4	11.8	6.4
Hylopetes sagitta (15512)	35.8	20.4	15.8	2.2	7.9	11.3	20.3	4.9	7.3	4.2	5.4	9.7	8.6	16.9	10.9	7.7
Glaucomys volans (19786)	34.4	28.3	16.0	2.0	7.3	8.3	20.8	4.7	6.3	4.4	5.0	10.0	9.8	15.7	10.4	7.4
Glaucomys sabrinus (IPS60584)	39.2	31.3	19.1	2.1	9.5	7.6	23.7	4.5	7.5	4.4	5.7	11.8	9.5	18.3	12.0	7.9
Iomys horsfieldii (15937)	30.5	23.8	15.7	1.1	5.7	8.3	19.1	5.1	7.2	2.8	4.8	8.3	7.4	15.7	8.6	7.2

TABLE 3. Endocranial volume, olfactory bulb, petrosal lobules, neocortical ratios and encephalization quotients for *Miopetaurista crusafonti* and published extant Pteromyini (Bertrand *et al.* 2017). To calculate the neocortical surface area ratio, we used the following formula NS1*2/TS. Volume and surface area ratios are expressed as percentages. The encephalization quotients were calculated using the equations of Eisenberg (1981) and Pilleri *et al.* (1984).

Subtribe	Species and specimen	Total endocast volume (cm^3)	Neocortical surface area ratio (%) NS1*2/TS	Olfactory bulb volume ratio (%)	Petrosal lobule volume ratio (%)	EQ (Eisenberg, 1981)	EQ Pilleri *et al.* (1984)
Pteromyina	*Miopetaurista crusafonti* (1978 V1)	10.82	30.19	1.21	1.92	1.01	1.13
Pteromyina	*Aeromys tephromelas* (USNM 481190)	11.46	35.19	2.85	1.45	1.35	1.45
Pteromyina	*Petaurista petaurista* (USNM 589079)	12.32	35.28	1.64	1.62	1.25	1.38
Pteromyina	*Pteromyscus pulverulentus* (USNM 481178)	3.62	33.82	2.81	1.37	1.32	1.23
Pteromyina	*Pteromys volans* (USNM 172622)	2.33	34.11	1.75	1.61	1.33	1.17
Glaucomyina	*Glaucomys volans* (AMNH 240290)	2.01	35.69	3.49	1.68	1.68	1.40
Glaucomyina	*Hylopetes spadiceus* (USNM 488639)	2.12	36.73	3.30	0.85	1.44	1.24
Glaucomyina	*Petinomys setosus* (USNM 488674)	1.51	35.76	3.10	-	1.73	1.38

TABLE 4. Phylogenetic generalized least-square linear regressions (PGLS) for endocast measurements and for total endocranial volume vs. body size in our sample (see Figs 9–10). For each regression, the values for the intercept, slope and associated significance, Pagel's λ, the pooled estimate of the residual standard error (RSE), degrees of freedom (df) for the model and residuals, 95 % confidence intervals for the slope (CI), and correlation coefficient (R^2) obtained from predicted and residual values. Residuals associated with the different regressions are provided in Grau-Camats *et al.* (2021, tables S6–S7). Body mass, olfactory bulb, petrosal lobule and endocast volume (in mm^3) as well as neocortical surface area for *Miopetaurista crusafonti* and other extinct and extant sciurid and ischyromyid rodents are given in Grau-Camats *et al.* (2021, table S4).

Equation	intercept	slope	p-value (slope)	λ	RSE	df	95% CI	R^2 (predicted)	R^2 (residuals)
Log (olfactory bulb volume) / Log (endocranial volume)	1.462	0.928	0.000	0.937	0.181	36, 34	[0.808, 1.049]	0.909	0.885
Log (olfactory bulb volume) / Log (body mass)	0.852	0.509	0.000	0.611	0.150	36, 34	[0.427, 0.592]	0.865	0.856
Log (neocortical surface area) / Log (endocranial surface area)	-0.405	0.981	0.000	1.014	0.111	36, 34	[0.923, 1.039]	0.939	0.905
Log (neocortical surface area) / Log (endocranial surface area) [excluding Ischyromyidae]	-0.430	0.998	0.000	-0.094	0.018	24, 22	[0.960, 1.036]	0.993	0.992
Log (petrosal lobule volume) / Log (endocranial volume)	-0.666	0.708	0.000	0.352	0.181	35, 33	[0.482, 0.933]	0.590	0.557
Log (petrosal lobule volume) / Log (body mass)	0.3461	0.292	0.006	0.396	0.221	35, 33	[0.151, 0.434]	0.401	0.356
Log (endocranial volume) / Log (body mass)	-0.531	0.488	0.000	0.429	0.104	36, 34	[0.427, 0.549]	0.897	0.889

1267